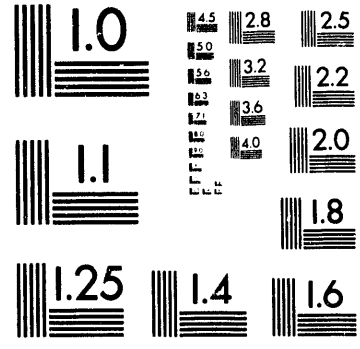
1.0
1.1
1.25
1.4
1.6
1.8
2.0
2.2
2.5
2.8
3.2
3.6
4.0
4.5
5.0
5.6
6.3
7.1
8.0
9.0

1 of 1

NUREG/CR-6079
RA

Seismological Investigation of Earthquakes in the New Madrid Seismic Zone

Final Report
September 1986–December 1992

Manuscript Completed: July 1993
Date Published: August 1993

Prepared by
R. B. Herrmann, B. Nguyen

Department of Earth and Atmospheric Sciences
Saint Louis University
3507 Laclede Avenue
St. Louis, MO 63103

Prepared for
Division of Engineering
Office of Nuclear Regulatory Research
U.S. Nuclear Regulatory Commission
Washington, DC 20555-0001
NRC FIN D1694
Under NRC Contract No. NRC-04-86-121

ABSTRACT

Earthquake activity in the New Madrid Seismic Zone had been monitored by regional seismic networks since 1975. During this time period over 3700 earthquakes have been located within the region bounded by latitudes 35° - 39°N and longitudes 87° - 92°W. Most of these earthquakes occur within a 1.5° x 2° zone centered on the Missouri Bootheel.

Source parameters of larger earthquakes in the zone and in eastern North America are determined using surface-wave spectral amplitudes and broadband waveforms for the purpose of determining the focal mechanism, source depth and seismic moment. Waveform modeling of broadband data is shown to be a powerful tool in defining these source parameters when used complementary with regional seismic network data, and in addition, in verifying the correctness of previously published focal mechanism solutions.

Table of Contents

List of Figures

List of Tables

Introduction

This report is the final report of work supported the U. S. Nuclear Regulatory Commission in order to monitor the earthquake process in the New Madrid Seismic Zone. Since seismic monitoring continues under U. S. Geological Survey support, databases are being maintained for future research. The thrust of this report is directed toward the analysis of larger earthquakes in the region from the point of view of developing techniques for analyzing broadband digital data that can be used as the USNRC supported U. S. National Seismic Network comes online. The report consists of four parts.

The first part applies a search technique to determine focal mechanisms from the surface-wave spectral amplitudes of earthquakes in the early 1980's in the eastern U. S. and Canada. The technique provides the five source parameters of dip, slip, strike, depth, and seismic moment through a combination of criteria requiring best correlation coefficients, least residuals between theoretical and observed spectral-amplitudes and equality between independent seismic moment estimates from Love and Rayleigh wave data.

This technique is applied to eight earthquakes of $m_b \approx 5$ that occurred in the North American continent in recent years. The focal mechanism results, constrained by P-wave first motions, indicate that near horizontal pressure axes are in the ENE-WSW for the 1982 Miramichi, New Brunswick (Canada) mainshock and one large aftershock (another large aftershock has ESE-WNW P-axis), the 1982 Gaza, New Hampshire mainshock, the 1982 Arkansas mainshock, the 1983 Goodnow, New York mainshock, and the 1986 Perry, Ohio mainshock. On the other hand a near horizontal tension axis in the direction NNE-SSW is found for the 1984 Wyoming mainshock in the western part of North American continent. The results obtained are consistent with the regional stress patterns and generally agree with the solutions of other investigators who used other aspects of the seismic wavefield.

The second section analyzes the New Madrid Seismic Zone earthquakes of September 26, 1990 and May 4, 1991 from the point of view of demonstrating how broadband digital recordings at regional distances can be used together with regional seismic network data to define source parameters and earth structure. Regional seismic network data provide excellent epicenter information and broadband data provide seismic moment values. In addition, the broadband data can provide strong constraints on both the focal mechanism when focal sphere coverage of regional network data is sparse and also the source depth when the epicenter is not well situated with respect to network geometry.

The September 26, 1990 earthquake has a source depth of 15 km, a seismic moment of $3\,x\,10^{22}$ dyne-cm. The focal mechanism is primarily one of thrust faulting, with the pressure axes aligned roughly E-W. One nodal plane strikes 140° and dips 75° to the SW and the other strikes 33° and dips 42° to the SE. The broadband waveform fit depth agrees well with aftershock monitoring.

The May 4, 1991 earthquake near Risco, Missouri had a source depth of 8 km well constrained by the PANDA deployment. The seismic moment is estimated to be $1.8 x 10^{22}$ dyne-cm. The focal mechanism indicates predominantly strike-slip faulting with P-axis trending NE-SW. One nodal plane strikes at 352° and dips 72° to the east, and the other strikes at 90° and dips 67.5° to the south.

Both focal mechanisms obtained are compatible with previous solutions in the seismic zone. In addition there is evidence of 3% variation in crustal velocities over slightly different paths.

The third section discusses the use of modern broadband, high resolution digital recording in making it possible to use waveform fit as a constraint for determining the focal mechanism, focal depth and seismic moment of small ($M_0 \approx 10^{22}$ dyne-cm) earthquakes in conjunction with some regional seismic network data. Examples of such a fit are show with the earthquakes of September 26, 1990 and May 4, 1991, which occurred within the environs of the New Madrid Seismic Zone. The orientation of focal mechanism pressure axes fit current models of mid-plate stress fields (Zoback and Zoback, 1991; Zoback, 1992).

Given the focal mechanism resolution inherent within the broadband waveforms, a re-examination of previously published focal mechanisms in the region is performed by comparing observed data with synthetics generated from published solutions. Two of the three published solutions which do not fit the accepted stress field are shown to be incorrect on the basis of waveform matching. These are the events of March 3, 1963 and July 21, 1967. The March 3, 1963 earthquake lies on a linear seismicity trend, and its revised mechanism agrees well with those of two other well defined earthquakes on the same trend.

Finally, the status of data acquired by the regional seismic network is discussed briefly in the last section.

SURFACE-WAVE FOCAL MECHANISMS

by B. V. Nguyen and R. B. Herrmann

INTRODUCTION

The estimation of source parameters has long been of special interest to seismologists. Ben-Menahem *et al.* (1968) described a procedure for obtaining the seismic source parameters from far-field radiation patterns through a search technique. Their search procedure used a set of measured equalized spectral amplitudes and fit them to a best pattern by minimizing the sum of the squares of the differences between the observed and theoretical spectral amplitudes for all periods as a function of the angles of dip, slip, and strike. Tsai and Aki (1969, 1970) used observed surface-wave amplitude spectra to determine focal depth, seismic moment and anelastic attenuation coefficients for some earthquakes using a known focal mechanism. They showed that the source spectrum could be adequately modeled by a step-source time function for periods between ten and fifty seconds and the finiteness factor may be neglected for earthquakes with M_S as large as 6.0 as long as source dimensions are no more than ten kilometers. Using a step function to represent the source time history, Tsai (1972) used observed surface-wave amplitude spectral data, corrected for instrument response and geometrical spreading, in the period range of 20 to 50 seconds and systematically searched through all possible focal mechanisms and depths in the crust and upper mantle until a set of optimum source parameters was found. The goodness of fit criteria required a solution that minimized the sum of the squares of all residuals between the observed and theoretical spectral values for both Love and Rayleigh waves together. The seismic moment is obtained in the process.

Following Tsai (1972), Herrmann (1974, 1979a) developed a search procedure using surface-wave spectral amplitude data. The best focal mechanism and focal depth combination was taken to be the one for which the correlation coefficients between the observed and theoretical spectral values for Rayleigh and Love waves are as large as possible and for which the seismic moment estimates for Rayleigh and Love waves are also as close as possible. The purpose of this was to maintain the independence of the data sets, since Love-wave spectral amplitudes can be significantly larger than those of Rayleigh waves for crustal events for some focal mechanisms. Nguyen (1985) modified the technique of Herrmann (1974, 1979a) to further automate the search.

SEARCH METHOD

For a given combination of the source depth and the strike, dip and slip angles, theoretical Rayleigh- and Love-wave spectra can be predicted at a given fixed reference distance and observation azimuth. In addition, knowledge of the anelastic attenuation of surface waves permits a correction for

this effect. We will define the spectral amplitude of the observed signal, corrected for geometrical spreading to a fixed reference distance and for anelastic attenuation, as Y_Q, and the corresponding theoretical prediction for a unit seismic moment as X_Q. These two quantities are related by the seismic moment, M_0 as

$$Y_Q = (M_0^Q)\, X_Q\,, \tag{1}$$

where the symbol Q is L for Love waves or R for Rayleigh waves.

The least squares estimate of the seismic moment is given by

$$M_0^Q = \frac{\sum_{j=1}^{N_Q} X_{Qj} Y_{Qj}}{\sum_{j=1}^{N_Q} X_{Qj}^{\,2}}\,, \tag{2}$$

where the j index refers to a particular (X_Q, Y_Q) pair, from the data set of all observed periods and azimuths. N_Q is the total number of observations of a particular wave type.

To estimate the source parameters, goodness of fit criteria are required. One criteria is very simple: the independent seismic moment estimates from the Love- and Rayleigh-wave data sets must agree. The second is that the predicted amplitudes match the observed. When viewing the data of a single period as a function of azimuth, this is equivalent to stating that the observed and theoretical radiation patterns agree in shape. This can be mathematically stated by defining a multi-dimensional vectors of the observations, $\mathbf{Y}_Q = (Y_{Q1}, Y_{Q2}, \ldots, Y_{QN_Q})$, and of the predictions, $\mathbf{X}_Q$. The goodness of fit estimate is just

$$R_Q = \frac{\mathbf{X}_Q \cdot \mathbf{Y}_Q}{|\mathbf{X}_Q|\,|\mathbf{Y}_Q|} \tag{3}$$

This is just the vector scalar product of unit vectors. Equation (3) is very similar to the correlation coefficient used in regression analysis, in that a +1 value indicates a perfect fit, but is better since it will work in the extreme case of a period independent, circular radiation pattern. For ease of discussion, we will use the term correlation coefficient to refer to this quantity.

One final goodness of fit parameter is the mean sum of squares of residuals defined as

$$RES_Q = \frac{1}{N_Q}\left[\sum_{j=1}^{N_Q}\left(Y_{Qj} - M_0 X_{Qj}\right)^2\right] \tag{4}$$

where $M_0 = \left(M_0^L + M_0^R\right)/2$. The separate estimates of RES_L and RES_R are made to avoid bias arising from the size of the data sets and also the size of the individual observations. Finally, all of these parameters can be combined

into a single goodness of fit parameter defined as

$$BEST = RATIO \frac{R_R R_L}{RES_R RES_L}, \quad (5)$$

where *RATIO* is the ratio of the individual seismic moment estimates, and is defined to be ≤ 1 .

To obtain a solution, a two step process is applied. The source parameter space of dip, slip and strike angles and source depth are systematically searched, computing values of RATIO and BEST for each combination. Since depth enters nonlinearly through the eigenfunctions, the solution method involves repeated searches at trial depths. For each trial depth in the search, the combination giving the largest value of BEST is retained as a candidate solution. In the second step, the preferred solution is the candidate solution that gives the largest value of RATIO. Because surface-wave amplitude spectra are used the fit is invariant to a rotation in the slip angle by 180°, and because of the invariance of the spectral amplitude radiation patterns to a rotation in the strike by 180° due to the use of a double-couple source, each solution from the search technique corresponds to four possible focal mechanisms. The choice of the final solution is constrained by the P-wave first motion data. If the selection criteria are relaxed slightly, e.g., by using a threshold on the RATIO and/or correlation coefficient values, then a suite of possible solutions arises, which can be used with the P-wave data to select a solution.

EARTHQUAKE DATA

The data were digitized from WWSSN (World Wide Standardized Seismograph Network) and CSSN (Canadian Standardized Seismograph Network) seismograms and were then transformed into the frequency domain for UZ (vertical), UR (radial), and UT (transverse) displacement components. Spectral amplitudes were normalized to a reference distance of 1000 km, and were corrected for geometrical spreading, instrument response, and anelastic attenuation using the results of Herrmann and Mitchell (1975). The multiple filter technique (MFT; Dziewonski *et al.,* 1969; Herrmann, 1973) was used to obtain smoothed modal spectral amplitude data and their associated group velocities. The analysis for source parameters employs the Central U.S. (CUS) crustal model (Herrmann *et al.,* 1980) and regional crustal models obtained by inversions of average Love-wave and Rayleigh-wave fundamental and first higher-mode group velocity data for the 1983 New York, 1984 Wyoming, and 1986 Ohio events. These events were also processed with frequency-variable, phase-matched filter (FVF, Russell *et al.,* 1988). Since for single station-single event analysis, the phase velocities can be ambiguous because of the unknown number of wavelengths between the source and receiver, the FVF phase velocity estimates will not be used. However the FVF technique also succeeds in isolating the signal of a single mode, and thus improves the spectral amplitude and group velocity dispersion estimate for an observation. Quality control was performed by comparing spectral

amplitudes observed 180° apart, which should theoretically be the same. In addition, spectral amplitude versus period plots were used to ensure that the observed spectra agreed with theoretical shapes (c.f., Tsai and Aki, 1970). Finally, since the MFT gave group velocity estimates associated with each spectral amplitude, data with extreme group velocites could be rejected.

The analysis for source studies employed vertical-component Rayleigh waves (UZ) and Love waves (UT). P-wave readings to constrain the nodal planes were read from various regional and teleseismic seismograms, when available.

Table 1 lists the epicenter and source data for the eight earthquakes studied.

Table 1
Epicenter and Source Data for Earthquakes Studied Using Surface Waves

ID	Area	Date	OT (UT)	Lat (°N)	Lon (°W)	m_b	M_S
1	NB	09 JAN 82	12 53 51.8	46.984	66.656	5.7	5.2
2	NB	09 JAN 82	16 36 42.9	47.023	66.648	5.1	3.9
3	NB	11 JAN 82	21 41 07.9	46.975	66.659	5.4	4.5
4	NH	19 JAN 82	00 14 42.0	43.500	71.600	4.5	-
5	AR	21 JAN 82	00 33 54.8	35.170	92.208	4.5	-
6	NY	07 OCT 83	10 18 46.1	43.938	74.258	5.1	-
7	WY	18 OCT 84	15 30 23.0	42.375	105.720	5.4	5.1
8	OH	31 JAN 86	16 46 43.3	41.650	81.162	5.0	-

This information is taken from the United States Geological Survey (USGS) Preliminary Determination of Epicenter (PDE). Table 2 lists general information of these events concerning data preparation and processing as well as P-wave first motion polarities in the order of increasing azimuth clockwise from North. The event number used is referenced to the corresponding entry in Table 1. As an example, for event 1, there are 174 Love wave spectral amplitude data points and 267 for Rayleigh. Fourteen stations provided Love-wave observations and nineteen provided Rayleigh-wave data. The processing filter employed was MFT. The spectral data set consisted of 20 periods in the range of 5 to 50 seconds. The P-wave first-motion polarity, (+) for compression, (-) for dilatation, and (X) for uncertain, is indicated for the stations used.

Miramichi, New Brunswick (Canada) Mainshock of 09 January 1982.

This is the largest event in our study. The stations that provided surface-wave data are shown in Figure 1a. The solution from the surface-wave search technique that satisfies the P-wave first motions is listed in Table 3 and shown in Figure 1b (solid pattern). The focal mechanism indicates predominant reverse dip-slip motions with smaller strike-slip components for both nodal planes. Using the CUS model, the value of the seismic moment is

Table 2
General Information About Data Set

ID	NL	NR	STATIONS L,R	FILTER Type	Periods Used	Period Range	P-Wave Polarity
1	174	267	14,19	MFT	20	5-50	ALE(+), STJ(-), GEO(+), BEV(+), AN4(X), IN3(+), JCT(+), AN8(+), AN3(+), BLO(+), AN7(X), AN9(+), FVM(-), IN1(-), LUB(+), DUG(+). BKS(-), LHC(-), SES(+), PHC(X), FCC(+), YKC(X), PMR(+), COL(+), FRB(-), SCH(-), AN10(+), AN11(-), AN12(+).
2	261	281	17,17	MFT	27	5-50	ALE(+), STJ(+), GEO(X), BLA(X), SHA(X), SCP(X), AN4(+), JCT(+), AN3(+), BLO(+), AN7(+), AN9(+), FVM(+), IN1(+), OTT(+), ANMO(+), DUG(+), LHC(X), SES(X), PNT(X), EDM(X), FFC(+), FCC(+), YKC(+), INK(+), MBC(+), FRB(-), SCH(X).
3	342	389	24,25	MFT	20	5-50	ALE(+), STJ(+), WES(X), GEO(X), BEV(X), BLA(+), IN3(+), JCT(X), AN3(+), BLO(X), AN10(+), AN9(X), AN12(+), IN2(-), IN1(+), AAM(X), MNT(+), OTT(X), DUG(+), SES(+), PNT(X), PHC(-), EDM(-), FFC(+), FCC(X), YKC(+), PMR(+), COL(+), INK(+), MBC(+), FRB(-), SCH(X).
4	69	72	4,6	MFT	20	5-50	SCH(-), WES(+), BLA(+), AAM(+), LHC(+), OTT(+), FFC(+), MNT(+), FCC(+),ONH(-), WNH(-), PNH(-), WFM(+), GLO(+), DUX(+), HNH(+), BVT(-), IVT(-),BNH(+), WES(+), QUA(+), NSC(-), DVT(+), LNX(+), UCT(+), HKM(+), HDM(+), MD1(+), ECT(+), BCT(-), EMM(+), PQ0(-), PQ1(+), HNME(-).
5	66	68	5,5	MFT	20	5-50	AAM(+), IN2(X), IN1(X), AN7(+), IN3(+), JCT(X), SES(+), EDM(X), FFC(+), FCC(+).
6	181	210	16,17	MFT,FVF	21	4-50	ALE(+), FRB(+), MNT(-), SCH(+), STJ(+), WES(+), BLA(+), SCP(-), JCT(+),FVM(-), AAM(+), ALQ(-), GOL(-), LON(+), SES(-), LHC(+), EDM(-), FFC(-), COL(+), INK(+), MBC(-).
7	222	334	12,17	MFT,FVF	21	4-50	ALE(-), FFC(-), SCH(+), OTT(-), AAM(-), SCP(-), BLA(+), FVM(-), SHA(+),JCT(+), LUB(-), GOL(+), ALQ(+), GSC(-), BKS(-), TID(+), CIB(-), TMI(-),HPI(-), KCI(+), JGI(+), GBI(-), IMW(-), LRM(-), BUT(-), MSO(-), SXM(-),HRY(-), COL(-), SES(+), EDM(-), INK(-), YKC(+), MBC(-).
8	273	311	15,16	MFT,FVF	21	4-50	FRB(+), JAQ(-), GSQ(-), EBN(-), BVT(-), QUA(-), WES(-), MD3(-), NSC(-),PAL(-), SCP(-), BLA(+), BAV(-), TRK(-), MGS(+), ZIN(+), LHS(+), VRN(+),GFM(+), PRM(+), BBG(+), TKL(+), DCT(+), GMG(-), ETT(X), RCT(-), RHT(+),TVG(-), HGA(-), BHT(-), PGM(+), IN4(-), OLY(+), AN4(-), BLO(-), AN3(-), AN1(-), FVM(-), SLM(+), IN2(-), AN7(-), AN9(-), IN1(-), GOL(-), CHI(-), DUG(-), HPI(-), IMW(-), JGI(-), ACM(-), EDM(+), YKC(+), MBC(+), PLVA(+), PKNC(+), BENN(X), BRBC(+), RICH(X), RBNC(X), SMTN(-), CCVA(X), GBTN(X), PKKY(+), L6KY(-), LGAR(+), SMKY(-), SFTN(X), AN10(-), AN11(-), AN12(-), LCNE(X), JAS1(-).

2.05×10^{24} dyne-cm for this mechanism for a focal depth of 9.5 km. For this solution, $RATIO$=0.999, R_L= 0.756, and R_R = 0.874.

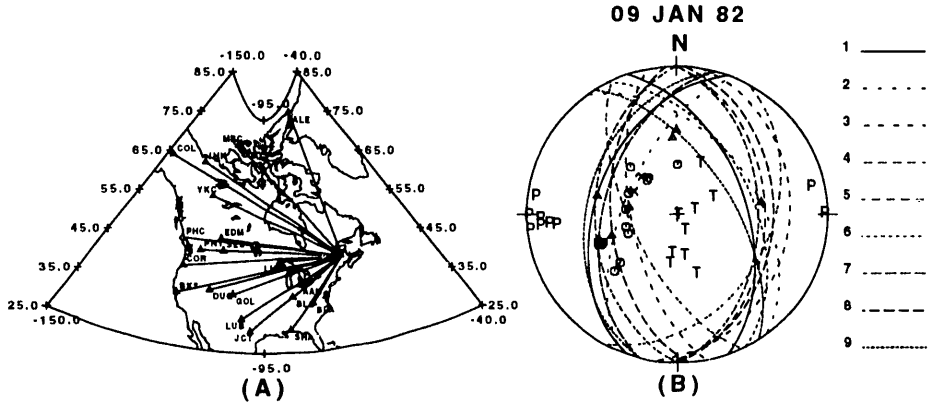

Fig. 1. (a) Location of seismograph stations used in surface-wave study of the Miramichi, New Brunswick (Canada) mainshock 09 January 1982. (b) Lower hemisphere projection of focal mechanism solutions of the Miramichi, New Brunswick mainshock 09 January 1982. P wave compressions, dilatations, and uncertainties are indicated by circles, triangles, and crosses, respectively. T and P indicate the orientation of the tension and pressure axes of the solution, respectively. DP1 (Dash Pattern 1, solid)=This study; DP2=Dziewonski and Woodhouse (1983); DP3=Choy *et al.* (1983); DP4=Choy *et al.* (1983); DP5=Hasegawa (1983)'s average values; DP6=Wetmiller *et al.* (1984); DP7=Suarez and Nábelek (1983); DP8=Nábelek (1985)'s best double couple; DP9=Yan and Alexander (1990).

The solution obtained is consistent with those given by Dziewonski and Woodhouse (1983) and Wetmiller *et al.* (1984). Additional focal mechanism results from other investigators (Choy *et al.*, 1983; Hasegawa, 1983; Suarez and Nábelek, 1983; Yan and Alexander, 1990) are tabulated in Table 3 and are basically consistent with this study.

Figure 2 compares plots of the predicted and observed spectral amplitudes at selected stations for Rayleigh waves (UZ) and Love waves (UT). The open squares are the equalized spectral amplitudes. The solid (this study) and dashed lines (other studies) are the predicted spectral amplitudes using the CUS crustal model. The match to the observed data using our solution is obviously better both in the level and shape of the spectral amplitudes for Rayleigh-wave data. Love-wave data for periods less than about 14 seconds are contaminated by off-axis Rayleigh-wave arrivals and possible lateral inhomogeneity in the paths of propagation. We match the spectral holes for Rayleigh-wave data well indicating that the depth of the source has been well obtained.

Miramichi Aftershock of 09 January 1982.

The stations that provided surface wave data are shown in Figure 3a. The solution from the surface-wave search technique that satisfies the P-wave first motion data is listed in Table 3 and shown in Figure 3b. The focal mechanism indicates a predominant reverse dip-slip motion with a small strike-slip component on the nodal plane striking NNW and a predominant dip-slip motion with a small strike-slip motion on the other plane striking SSW. The solution has a focal depth of 6.0 km in the CUS crustal model with the value

Table 3
Summary of Focal Mechanism Parameters For Earthquakes Studied

ID	m_b	Date	Dip	Slip	Strike	M_0 (dyne-cm)	H (km)	Authors
				Miramichi, New Brunswick (Canada) Mainshock 09 January 1982				
1	5.7	01/09/82	45.0	120.0	200.0	$2.05x10^{24}$	9.5	This study
			50.0	120.0	195.0	$2.20\pm0.70x10^{24}$	7.0	Wetmiller *et al.* (1984)
			65.0	60.0	155.0	$4\text{-}6.60x10^{24}$	9.0	Choy *et al.* (1983)
			65.0	81.0	169.0	$3.20x10^{24}$	9.0	Choy *et al.* (1983)
			47.0	42.0	324.0	$2.00x10^{24}$	10.0	Dziewonski and Woodhouse (1983)
			35.0-65.0	70.0-130.0	185.0-205.0	$1.50\text{-}6.00x10^{24}$	6.0-10.0	Hasegawa (1983)
			45.0	90.0	180.0	$1.10x10^{24}$	-	Suarez and Nábelek (1983)
			54.0	86.0	176.0	$1.60x10^{24}$	7.0	Nábelek (1985)'s best double couple
			40.0	130.0	195.0	-	7.0	Yan and Alexander (1990) station SCP
				Miramichi, New Brunswick Aftershock 09 January 1982				
2	5.1	01/09/82	60.0	130.0	215.0	$1.55x10^{23}$	6.0	This study
			50.0	130.0	195.0	-	6.0	Yan and Alexander (1990) station SCP
				Miramichi, New Brunswick Aftershock 11 January 1982				
3	5.4	01/11/82	60.0	125.0	200.0	5.86+23	7.5	This study
			40.0	80.0	342.0	-	6.0	Yan and Alexander (1990) station SCP
			53.0	108.0	332.0	$4.20x10^{23}$	7.0	Nábelek (1985)'s best double couple
				Gaza, New Hampshire Mainshock 19 January 1982				
4	4.5	01/19/82	35.0	120.0	200.0	$2.69x10^{22}$	8.0	This study
			30.0	120.0	195.0	$2.75x10^{22}$	4.0	This study
			33.2	114.1	193.2	$3.12x10^{22}$	11.0	This study
			39.0	70.0	344.0	-	-	Ebel and Bouck (1988)
			68.0	200.0	19.0	-	-	Sauber (1985)
			80.0	162.0	20.0	$3.00x10^{22}$	3.4	Pulli *et al.*(1983)
				Arkansas Mainshock 21 January 1982				
5	4.5	01/21/82	60.0	55.0	330.0	$4.73x10^{22}$	6.0	This study
				Goodnow, New York Mainshock 07 October 1983				
6	5.1	10/07/83	70.0	115.0	170.0	$2.24x10^{23}$	9.0	This study
			24.0	71.0	343.0	$3.0x10^{23}$	28.3±12.9	Harvard CMT (PDE)
			31.0	106.8	19.5	$2.5x10^{23}$	7.3	Toksoz and Pulli (1984)
			30.0	60.0	316.0	$2.0x10^{23}$	7.0	Seeber and Armbruster(1986)
			30.3	105.8	18.1	$1.9x10^{23}$	7.5	Nábelek and Suarez (1989)
				Wyoming Mainshock 18 October 1984				
7	5.4	10/18/84	60.0	335.0	350.0	$9.33x10^{23}$	25.0	This study
			51.0	225.0	270.0	$1.10x10^{24}$	21.9±4.3	Harvard CMT (PDE)
			79.1	335.4	333.7	-	24.0	Gordon and Needham (in Langer, 1985). Depth by Tarr (1985)
				Perry, Ohio Mainshock 31 January 1986				
8	5.0	01/31/86	80.0	165.0	25.0	$1.11x10^{23}$	6.0	This study
			72.0	6.0	115.0	$3.40x10^{23}$	15.0	Harvard CMT (PDE)
			73.0	171.0	55.0	-	-	NEIS by Needham (in Nicholson *et al.*, 1988)

of the seismic moment being 1.55×10^{23} dyne-cm. For this solution *RATIO* = 0.998, R_L = 0.564, and R_R = 0.755.

The focal mechanism result obtained by Yan and Alexander (1990) from just two or three GDSN stations is in good agreement with the result of this study. They used a surface-wave L/R spectral ratio technique. Their mechanism for this station is plotted in Figure 3b and tabulated in Table 3.

Miramichi Aftershock of 11 January 1982.

The stations that provided surface wave data are shown in Figure 4a. The solution from the surface-wave search technique that satisfies the P-wave first motions is listed in Table 3 and shown in Figure 4b. The focal mechanism indicates a predominant reverse dip-slip motion with a small strike-slip component on the nodal plane striking NNW. The mechanism was found at a

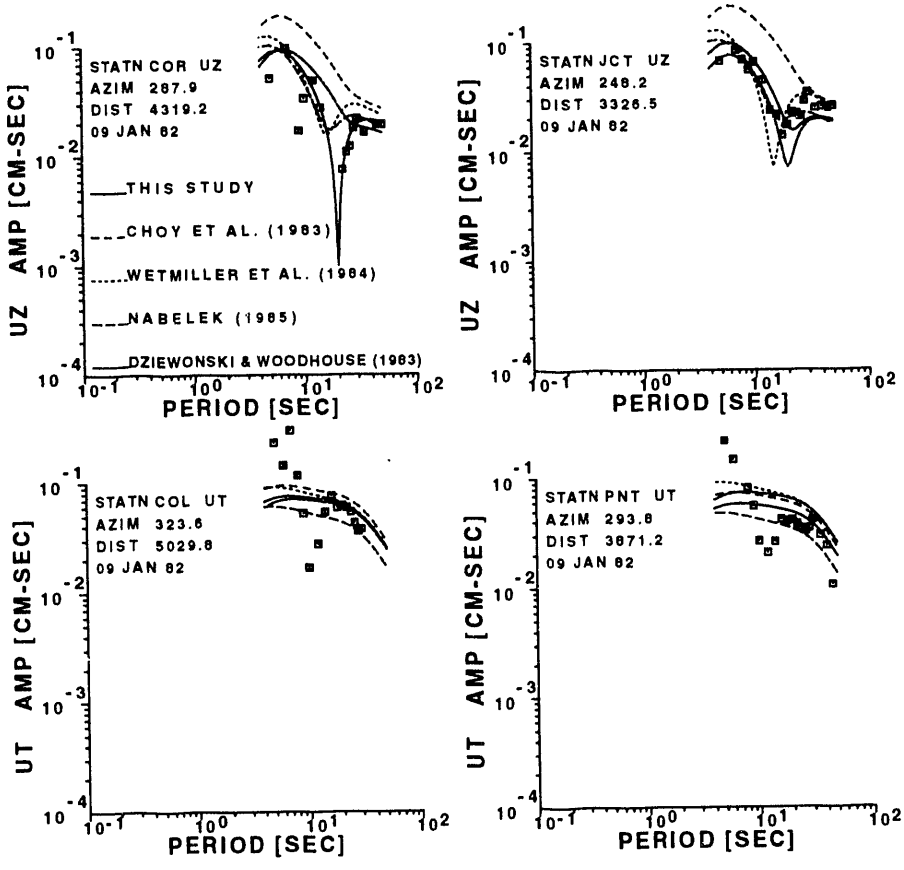

Fig. 2. Predicted (solid and dashed lines) and observed (squares) spectral amplitudes for some selected stations (UZ=Rayleigh waves, UT=Love waves) of the Miramichi, New Brunswick mainshock. Eigenfunctions were computed from the CUS crustal model. Source parameters are from this study and from others.

focal depth of 7.5 km in the CUS model with the value of the seismic moment being 5.86×10^{23} dyne-cm. For this solution, $RATIO = 0.999$, $R_L = 0.709$ and $R_R = 0.867$.

Additional focal mechanism results by other investigators (Nábelek, 1985; Yan and Alexander, 1990) are consistent with our solution. Their focal mechanisms are plotted in Figure 4b and tabulated in Table 3.

Figure 5 shows our predicted and the observed spectral amplitudes for Love waves (UT) and for Rayleigh waves (UZ) at selected stations. The observed data for Love waves at periods less than 14 seconds are noisy. The Rayleigh waves are contaminated by noise and possible lateral inhomogeneity at periods less than about 7-8 seconds. Except for this, the match of our predicted spectral amplitudes to the observed are excellent. The agreement between the observed and our predicted Rayleigh-wave spectral holes indicates that the depth of the source has been well obtained and also that focal mechanism

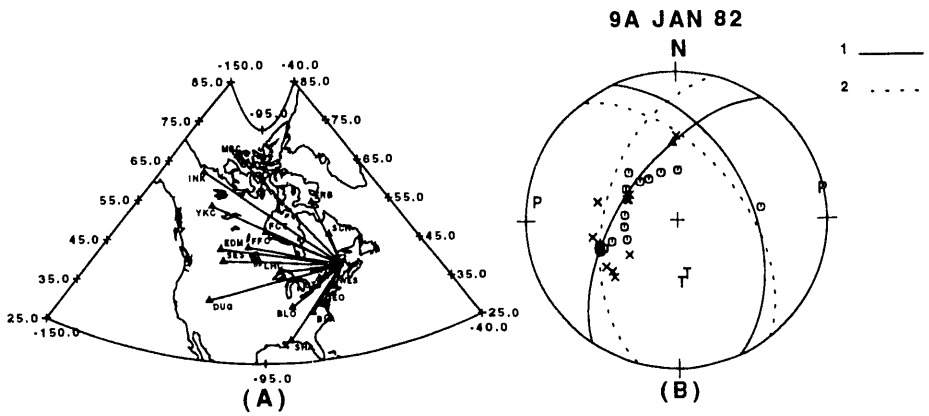

Fig. 3. (a) Location of seismograph stations used in surface-wave study of the Miramichi, New Brunswick aftershock 09 January 1982. (b) Lower hemisphere projection of focal mechanism solutions of the New Brunswick aftershock 09 January 1982 with annotations explained in Figure 1b. DP1 (Dash Pattern 1)=This study; DP2=Yan and Alexander (1990).

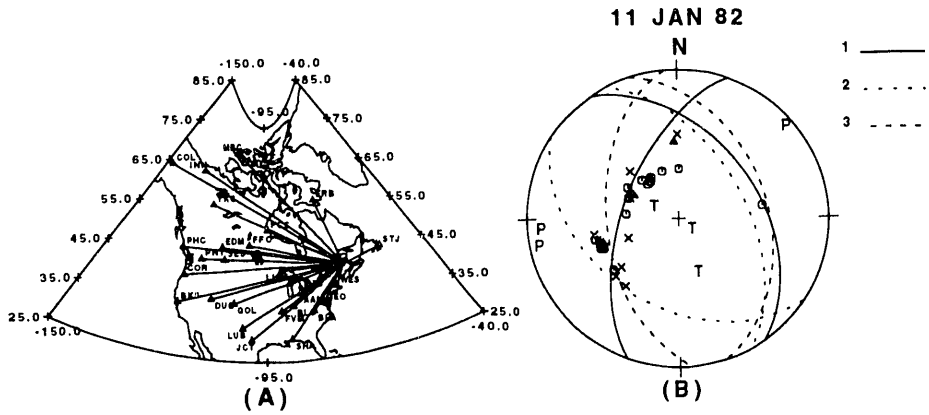

Fig. 4. (a) Location of seismograph stations used in surface-wave study of the Miramichi, New Brunswick aftershock 11 January 1982. (b) Lower hemisphere projection of focal mechanism solution of the Miramichi, New Brunswick aftershock 11 January 1982 with annotations explained in Figure 1b. DP1 (Dash Pattern 1)=This study; DP2=Nábelek (1985)'s best double couple; DP3=Yan and Alexander (1990).

is almost pure 45° dip slip. The predicted spectral amplitudes from Nábelek (1985)'s solution does not fit the the observed Love and Rayleigh-wave spectral amplitude data well, showing the sensitivity of the surface-wave data to strike.

Gaza, New Hampshire Earthquake of 19 January 1982.

For this smaller event, only 4 stations had usable Love-wave data, and 6 had Rayleigh-wave data (Table 3). However, the 180° azimuthal coverage about the source is adequate. The stations that provided surface-wave data are shown in Figure 6a. The focal mechanism obtained indicates predominant reverse dip-slip motions. The value of the seismic moment is $2.69 x 10^{22}$

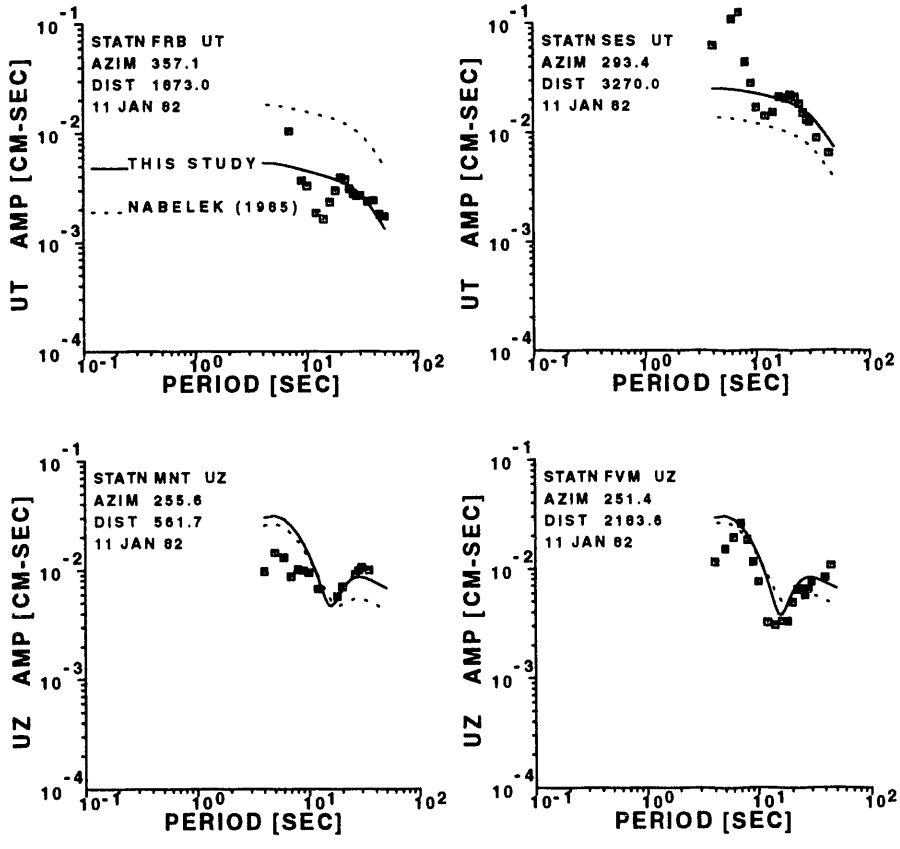

Fig. 5. Predicted (solid and dashed lines) and observed (squares) spectral amplitudes for some selected stations (UT=Love waves, UZ=Rayleigh waves) of the Miramichi, New Brunswick aftershock 11 January 1982. Eigenfunctions were computed from the CUS crustal model. Source parameters are from this study and from others.

dyne-cm for this mechanism at a focal depth of 8.0 km in the CUS model. The *RATIO* value is 0.997, R_L is 0.876, and R_R is 0.865. The search technique indicated that depth of 4 km or 11 km also provide acceptable fits to the limited spectral amplitude data. The focal mechanism results remain essentially the same at these depths as the focal mechanism result at 8 km. The solutions from the surface-wave search technique at depths 4 km, 8 km, and 11 km, constrained by the P-wave first motions, are listed in Table 3 and shown in Figure 6b. The solutions given by other investigators are also plotted in this figure.

Figure 7 shows predicted and observed spectral amplitudes. The match to the observed data from the dip-slip results of this study at depths of 4 km, 8 km, and 11 km is much better than that from the strike-slip result of Pulli *et al.,* (1983) both in the level and shape of the spectral amplitudes.

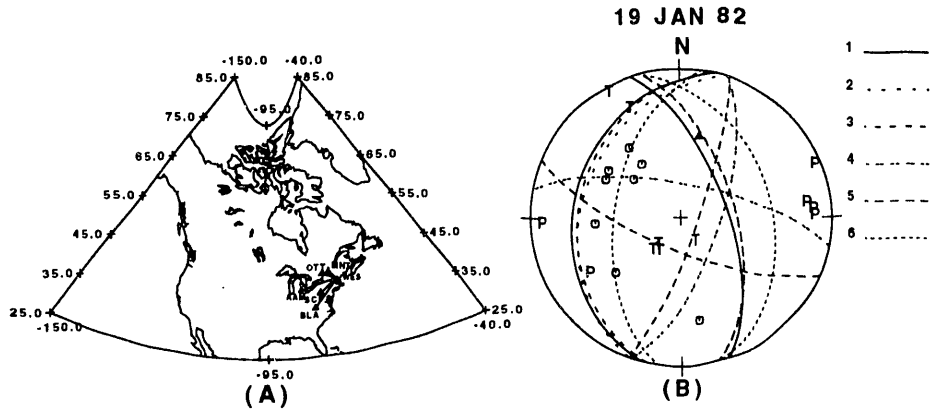

Fig. 6. (a) Location of seismograph stations used in surface-wave study of the Gaza, New Hampshire mainshock 19 January 1982. (b) Lower hemisphere projection of focal mechanism solutions of the Gaza, New Hampshire mainshock 19 January 1982 with annotations explained in Figure 1b. DP1 (Dash Pattern 1)=This study at 4 km depth; DP2=This study at 8 km depth; DP3=This study at 11 km depth; DP4=Sauber (1985); DP5=Pulli *et al.* (1983); DP6=Ebel and Bouck (1988).

Due to the significant difference between our solutions and that of Pulli *et al.* (1983), a hypocentral relocation program (Herrmann, 1979b) was used to relocate this event with a total of 25 short-period P-wave arrival times obtained from analog playbacks of digital records of the Massachusetts Institute of Technology and from microfilm recordings of Weston Observatory-Boston College seismic networks. The additional 25 P-wave first motions are tabulated in Table 2. The New England (WES) velocity model (in Foley *et al.*, 1982) was used in the hypocentral relocation. The results are tabulated in Table 4 along with the location results by NEUSSN.

Table 4
Location of 19 January 1982 Event

	NEUSSN	This Study
RMS Eerror	0.310	0.239
Origin Time	00:14:42.67±0.31	00:14:42.67±0.09
Depth	7.41±1.2 km	8.07±0.96 km
Latitude	43.508N	43.509±0.004N
Longitude	71.619W	71.631±0.007W
Epicentral Error	0.9 km	-
Semi-major Axis	-	0.64 km
Semi-minor Axis	-	0.44 km
Trend of minor Axis	-	N27.25°E

The new results are much improved in the RMS error.

Figure 8a shows the location of these stations about the epicenter. Since the relocation results did not affect the previous travel times used for long-period surface wave analysis (e.g., the same time window for digitization), the results for the surface-wave focal mechanism remain valid with respect to the

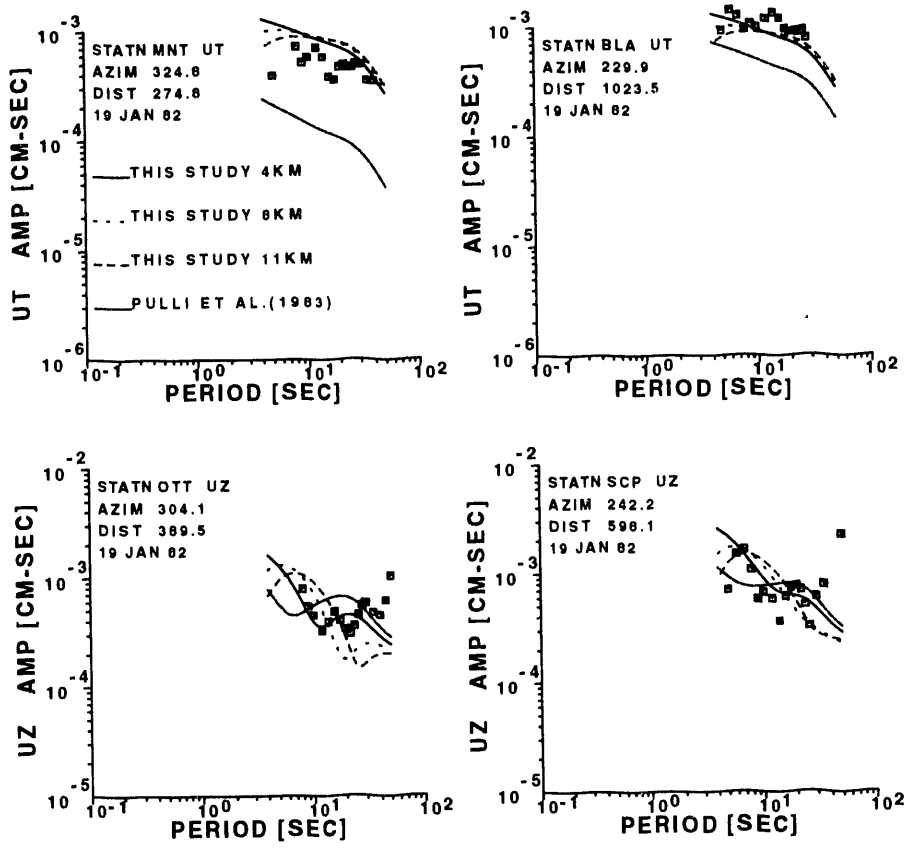

Fig. 7. Predicted (solid and dashed lines) and observed (squares) spectral amplitudes for some selected stations (UZ=Rayleigh waves, UT=Love waves) of the Gaza, New Hampshire mainshock 19 January 1982. Eigenfunctions were computed from the CUS crustal model. Source parameters at various depths from this study and from Pulli *et al.*(1983).

newly relocated epicenter values. However the relocation introduced different takeoff angles for P waves as a result of the inclusion of various earth models for different types of data involved in the focal mechanism plot. As such, there was a need for revised surface-wave focal mechanism estimates. There were 146 combinations of dip, slip, and strike of the original search for a depth equal to 8 km that satisfied two strong criteria:

(a) the ratio of seismic moments of independent Love and Rayleigh wave estimates equals or exceeds 0.99 for a given focal mechanism;

(b) the correlation coefficients for Love waves (RL) as well as for Rayleigh waves (RR) equal or exceed 0.8.

Of these 146 combinations, there exists a total of 584 combinations (146 x 4) that satisfy exactly the above prescribed two criteria, due to surface-wave 180° spectral invariance. Since the solution at 8 km for this event is still

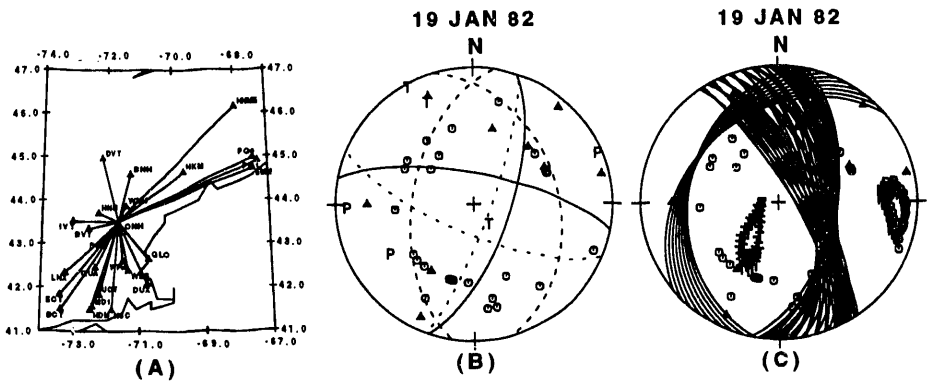

Fig. 8. (a) Map of the relocated epicenter and 25 short-period P-wave stations used in the relocation of the Gaza, New Hampshire mainshock 19 January 1982. (b) Lower hemisphere projection of focal mechanism solutions by other authors with the additional 25 short-period P-wave first motions after a source relocation. The strike-slip mechanisms of of Pulli *et al.* (1983) (spaced dashed lines) or Sauber (1985) (solid lines) are less compatible with the P-wave first motions than the dip-slip mechanism of Ebel and Bouck (1988) (dashed lines). (c) same as (b) but with 48 combinations of surface-wave focal mechanism at depth of 8 km by this study, which provide better compatibility with P-wave first motions and which indicate that our previous surface-wave focal mechanism at this depth still holds after a source relocation.

valid, that solution is used as a master model to select solutions with dip fixed at 35°, slip between 75° to 165°, and strike between 155° to 245°. Of the 584 combinations, only 48 combinations were within these ranges. These 48 combinations, including the solution at 8 km depth for the New Hampshire event, are shown in Figure 8c. Figure 8b indicates that if the strike-slip focal mechanism given by Pulli *et al.* (1983) or Sauber (1985) were used to fit these P-wave first motions, the strike-slip mechanism would be inadequate to simultaneously fit the surface-wave data. It should be noted that the first motions used here account for the correct sense of first motion on the sensors. These polarity reversals were first noted by Nguyen (1985) while plotting synthetic seismograms for this event and were later acknowledged by Ebel and Bouck (1988). Their focal mechanism result for this event is in good agreement with ours. The focal mechanism given by Ebel and Bouck is also plotted in Figure 8b.

Arkansas Main Event of 21 January 1982.

A total of 5 stations for Love waves and 5 stations for Rayleigh waves were used in the analysis (Table 2). The stations that provided surface wave data are shown in Figure 9a. the P-wave first motions is listed in Table 3 and shown in Figure 9b. The focal mechanism indicates a predominant reverse dip-slip motion on the nodal plane striking NNW. For this mechanism in the CUS model at a focal depth of 6.0 km, the value of the seismic moment is $4.73 x 10^{22}$ dyne-cm. The *RATIO* value is 0.999, R_L is 0.731, and R_Q is 0.841. It should be noted that most of the signals for this event were observed to be overridden by some teleseismic signals at very long periods. However, the focal mechanism can still be obtained by the search technique.

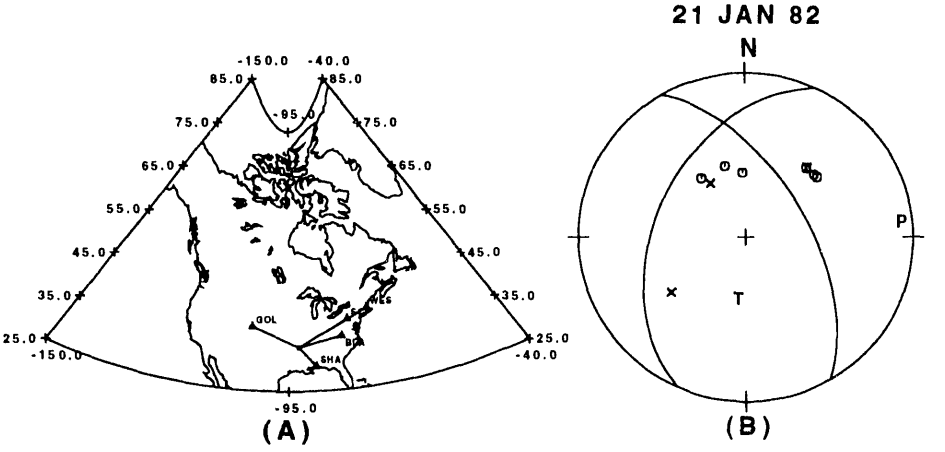

Fig. 9. (a) Location of seismograph stations used in surface-wave study of the Arkansas mainshock 21 January 1982. (b) Lower hemisphere projection of focal mechanism solution for the Arkansas mainshock 21 January 1982 with annotations explained in Figure 1b.

Johnston (1982) estimated a swarm source area of 6 km by 6 km. The source depth predicted as 6 km is within Johnston's source volume location between 1 and 9 km deep. He also hypothesized the cause of the swarm as a reactivation of existing faults by the intrusion of a small magma body. Chiu *et al.* (1984) compiled 88 events of the 1982 Arkansas swarm during a 12-day period. These events occurred within a small volume of about 45 km^3 at depths from 4 to 7 km. Their composite focal mechanisms indicate predominant strike-slip motion with the P axis oriented NE-SW. Saikia and Herrmann (1986) used waveform matching techniques to estimate focal mechanisms and seismic moments of three aftershocks recorded at short distances. They found a P-axes with NE-SW to NW-SE orientations, and three different mechanisms: one roughly a north striking strike-slip, one a north striking thrust mechanism, and one a northeast striking normal event.

Because of the poor station coverage and poor signal to noise ratio for the mainshock analyzed in this study, we assign our event quality as C, with A being best (Table 5, c.f. Herrmann, 1979a). We suggest, on the basis of available data analysis, that the mainshock was reactivated by a predominant dip-slip motion with a small strike-slip component on the nodal plane striking NNW (this study), followed by predominant strike-slip aftershocks (Johnston, 1982; Chiu *et al.*, 1984).

Goodnow, New York Mainshock of 07 October 1983.

The stations that provided surface wave data are shown in Figure 10a. The crustal model used in the final determination of source parameters was derived by inverting the mean observed first higher mode and fundamental mode Love-wave and Rayleigh-wave group velocities. For reference with the CUS model, the shear structure is tabulated in Table 6 of the last section and shown in Figure 17.

Table 5
Surface-Wave Source Parameter Summary

ID	Date	Dip (°)	Slip (°)	Stk (°)	T-axis (Trn, Pln)	P-axis (Trn, Pln)	M_o (dyne-cm)	H (km)	m_b	M_S	QUAL†
1. NB	01/09/82	45	120	200	(189,69)	(89,4)	2.05×10^{24}	9.5	5.7	5.2	A
		52	63	341							
2. NB	01/09/82	60	130	215	(178,55)	(278,7)	1.55×10^{23}	6.0	5.1	3.9	A
		48	42	336							
3.NB	01/11/82	60	125	200	(162,59)	(266,9)	5.86×10^{23}	7.5	5.4	4.5	A
		45	45	325							
4. NH	01/19/82	35	120	200	(215,69)	(89,13)	2.69×10^{22}	8.0	4.5		B-
		60	71	345							
5. AR	01/21/82	60	55	330	(189,59)	(84,9)	4.73×10^{22}	6.0	4.5		C
		45	135	205							
6. NY	10/07/83	70	115	170	(114,58)	(241,21)	2.24×10^{23}	9.0	5.1		A
		32	41	296							
7. WY‡	10/18/84	60	335	350	(220,5)	(314,38)	9.33×10^{23}	25.0	5.4	5.1	A-
		69	213	93							
8. OH	01/31/86	80	165	25	(341,18)	(72,3)	1.11×10^{23}	6.0	5.0		A
		75	10	118							

† Refers to data quality and station coverage with A=best.
‡ Western part of North American continent.

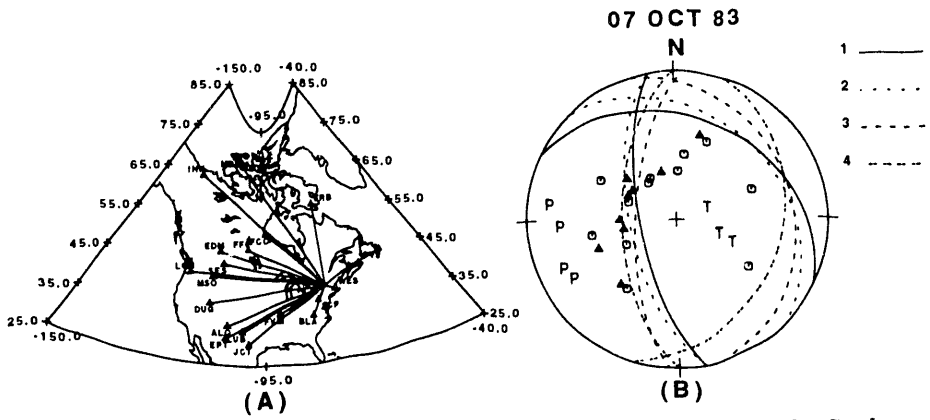

Fig. 10. (a) Location of seismograph stations used in surface-wave study of the Goodnow, New York mainshock 07 October 1983. (b) Lower hemisphere projection of focal mechanism solutions for the Goodnow, New York mainshock 07 October 1983 with annotations explained in Figure 1b. DP1 (Dash Pattern 1)=This study; DP2=Seeber and Armbruster (1986); DP3=Harvard CMT (PDE); DP4=Toksöz and Pulli (1984), Nábelek and Suarez (1989).

The solution from the surface-wave search technique that satisfies the P-wave first motions is listed in Table 3 and shown in Figure 10b. The focal mechanism indicates predominant reverse dip-slip motions with smaller strike-slip components for both nodal planes. For this mechanism at a focal depth of 9.0 km in this crustal model, the value of the seismic moment is 2.24×10^{23} dyne-cm. The *RATIO* value is 0.999, R_L is 0.856, and R_R is 0.910.

Our solution is in good agreement with the fault plane solution of Seeber and Armbruster (1986). The depth of about 7 km given by them was referenced to the depth given by Suarez *et al.* (1984). A composite focal mechanism for the aftershocks of the New York event was compiled by Seeber and Armbruster (1986) which shows a mechanism similar to the mainshock. In general, reverse faulting was found by them for the two nodal planes. Additional focal mechanism results obtained by Toksöz and Pulli (1984), Nábelek and Suarez (1989) are also consistent with the result of this study.

Figure 11 shows our predicted and observed spectral amplitudes for Love

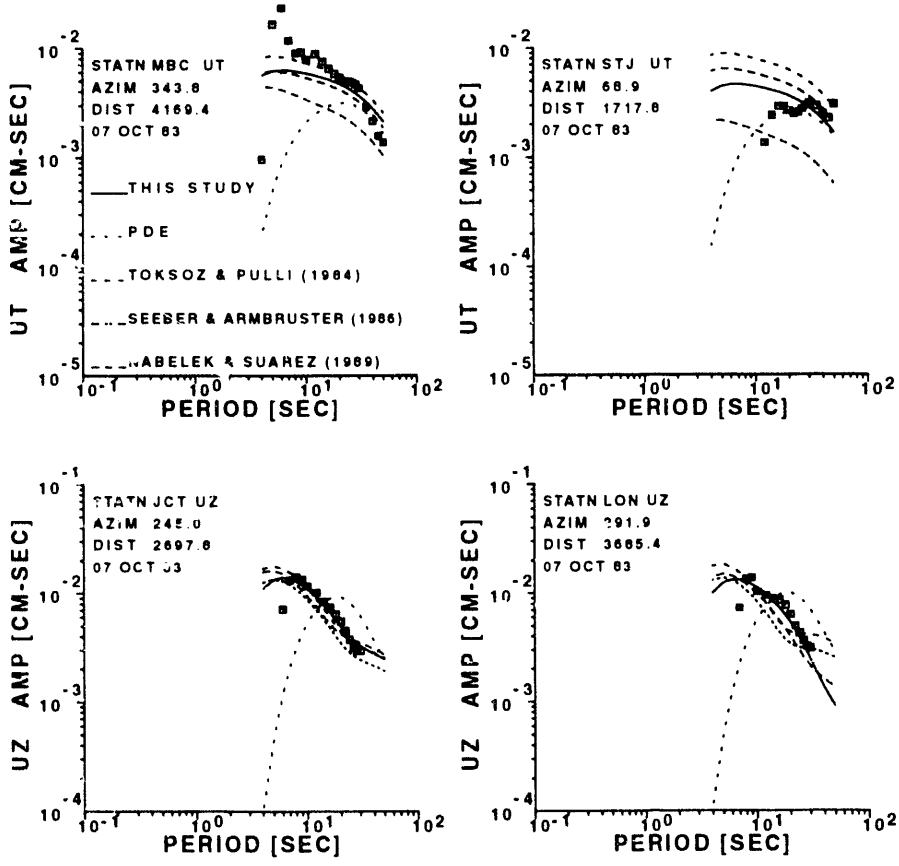

Fig. 11. Predicted (solid and dashed lines) and observed (squares) spectral amplitudes for some selected stations (UT=Love waves, UZ=Rayleigh waves) of the Goodnow, New York mainshock 07 October 1983. Eigenfunctions were computed from the crustal model obtained by inversion (Table 6, Columns 1 and 2; Figure 17). Source parameters are from this study and from others.

waves (UT) and Rayleigh waves (UZ). We obtain good matches to the observed spectral amplitudes both in the level and the shape. For Love waves, the data of periods less than about 14 seconds are noisy. The depth of 28.3 km given in the PDE from the Harvard CMT solution is not constrained and is too deep, as is seen by the poor fit to observed spectra at short periods.

Liu *et al.* (1991) determined the focal mechanisms of five small aftershocks by waveform modeling of aftershocks recorded at short distances, and found that three aftershocks had focal mechanisms similar to our surface-wave solution.

Wyoming Mainshock of 18 October 1984 The stations that provided surface wave data are shown in Figure 12a.

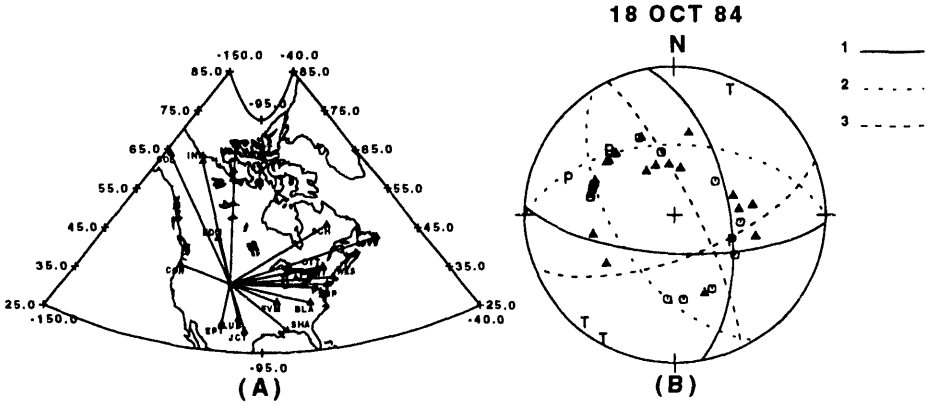

Fig. 12. (a) Location of seismograph stations used in surface-wave study of the Wyoming mainshock 18 October 1984. (b) Lower hemisphere projection of focal mechanism solutions for the Wyoming mainshock 18 October 1984 with annotations explained in Figure 1b. DP1 (Dash Pattern 1)=This study; DP2=Harvard CMT (PDE); DP3=Gordon and Needham (in Langer, 1985).

The crustal model employed came from the inversion of average Love-wave and Rayleigh-wave first higher mode and fundamental mode group velocities (Table 6, Figure 17).

The solution from the surface-wave search technique that satisfies the P-wave first motions is listed in Table 3 and shown in Figure 12b. The focal mechanism indicates predominant strike-slip motion with smaller normal dip-slip motion on both nodal planes. For this mechanism at a focal depth of 25.0 km in this crustal model, the value of the seismic moment is 9.33×10^{23} dyne-cm. The RATIO value is about 1.0. The correlation coefficient for Love waves is 0.903; for Rayleigh waves, 0.744.

The solution obtained is consistent with that given by Gordon and Needham (reported by Langer, 1985). Tarr (1985) estimated a depth of 24 km for this event and depths of 21 to 24.5 km for 14 aftershocks. According to Langer (1985), the epicentral locale for most of the aftershocks is within a 13 km^2 area. Depths extend from about 21.0 to 25.5 km with the deepest events occurring in the southern part of the aftershock zone. Focal mechanism solutions were determined for 45 of the 49 located aftershocks and indicate normal and strike-slip modes of faulting. In all cases, the location of the T-axes is near horizontal and they trend to the northeast at about the same angle as the T-axis of the mainshock.

The focal mechanism given by the Harvard CMT (PDE) would be compatible with the fault plane solution given by Gordon and Needham or to the one

determined in this study if its strike were changed by 180° with a slight increase in dip angles.

Figure 13 shows spectral amplitudes of the observed and

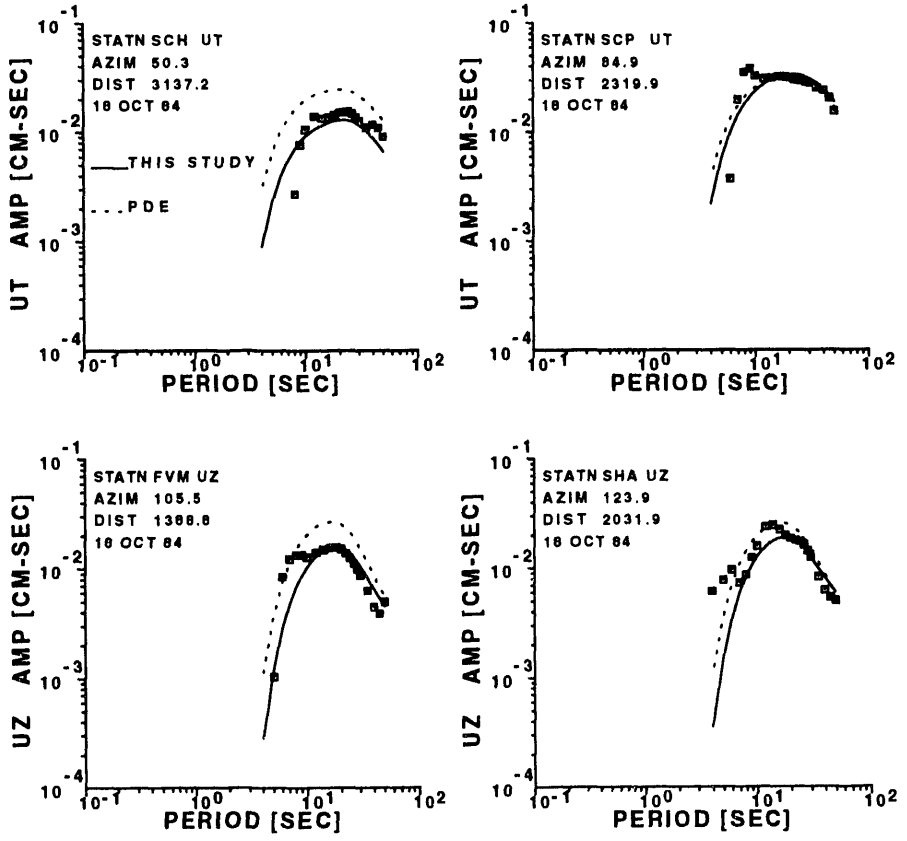

Fig. 13. Predicted (solid and dashed lines) and observed (squares) spectral amplitudes for some selected stations (UT=Love waves, UZ=Rayleigh waves) of the Wyoming mainshock 18 October 1984. Eigenfunctions were computed from the crustal model obtained by inversion (Table 6, Columns 1 and 3; Figure 17). Source parameters are from this study and from Harvard CMT (PDE).

the predicted for Love waves (UT) and Rayleigh waves (UZ). The match of our predicted spectral amplitudes (solid lines) to the observed are superb both in the level and the shape. Data for Love waves are noisy or due to possible lateral inhomogeneity along propagation paths at periods less than about 14 seconds. The predicted spectral amplitudes for the Harvard CMT focal mechanism (dashed lines) tend to be higher than the observed.

Perry, Ohio Mainshock 31 January 1986.

The stations that provided surface wave data are shown in Figure 14a. The crustal model use was obtained by inversion of average Love-wave and Rayleigh-wave first-higher-mode and fundamental-mode group velocities

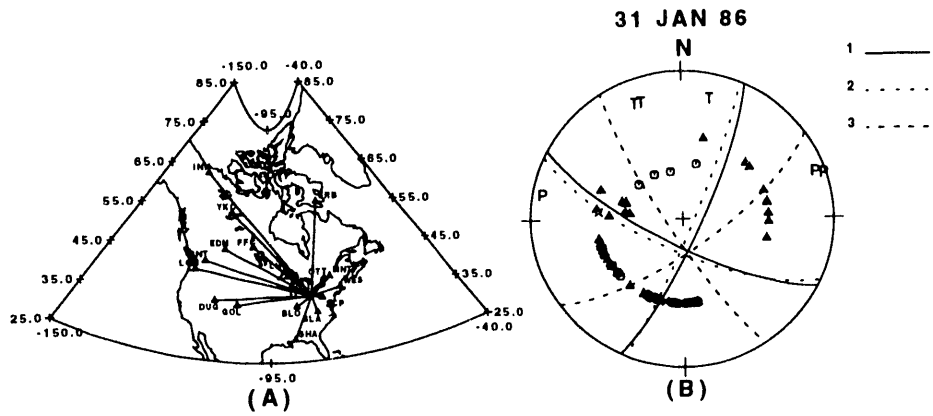

Fig. 14. (a) Location of seismograph stations used in surface-wave study of the Perry, Ohio mainshock 31 January 1986. (b) Lower hemisphere projection of focal mechanism solutions for the Perry, Ohio mainshock 31 January 1986 with annotations explained in Figure 1b. DP1 (Dash Pattern 1)=This study; DP2=Harvard CMT (PDE); DP3=NEIS by Needham (in Nicholson *et al.*, 1988).

(Table 6, Figure 17). The solution from the surface-wave search technique that satisfies the P-wave first motions is listed in Table 3 and shown in Figure 14b. The seismic moment and depth are $1.11 x 10^{23}$ dyne-cm and 6 km. The *RATIO* value is 0.999, R_L = 0.826 and R_R = 0.851.

The focal mechanism result indicates predominant strike-slip motions with much smaller reverse dip-slip motions on both nodal planes. The result obtained is in excellent agreement with Harvard Centroid Moment Tensor Solution listed in the PDE. The source depth given by the PDE, however, is not constrained but fixed at 15 km. The fault plane solution given by Needham in NEIS (Nicholson *et al.*, 1988) shows a strike differing by about 35° clockwise from the result of this study. Nicholson *et al.* (1988) estimated focal depths of the aftershocks of magnitudes of 0.5 to 2 to range to be 2 to 6 km. Focal mechanisms of the aftershocks exhibit predominantly oblique right-slip motion on nearly vertical nodal planes oriented N15°E to N45°E, with a nearly horizontal P axis north or east. Mrotek *et al.* (1986) reports that the aftershocks form a linear trend striking approximately N20°E with a length of about 3 km. Their composite fault plane solution based on 33 first motions from 7 events indicates either right-lateral strike-slip motion on a NNE striking plane, or left-lateral faulting on an ESE striking plane. The direction of maximum compressive stress inferred from the fault plane solution is ENE. Focal depths of these aftershocks were calculated to lie between about 2.5 km and 8.0 km.

Figure 15 shows our predicted (solid lines) and observed (open squares) spectral amplitudes for Rayleigh waves (UZ) and Love waves (UT). The predicted spectral amplitudes match the observed well. They also match the observed spectral holes in Rayleigh-wave plots (e.g., MNT UZ) indicating the depth of the source is well constrained. On the other hand, the levels of the predicted

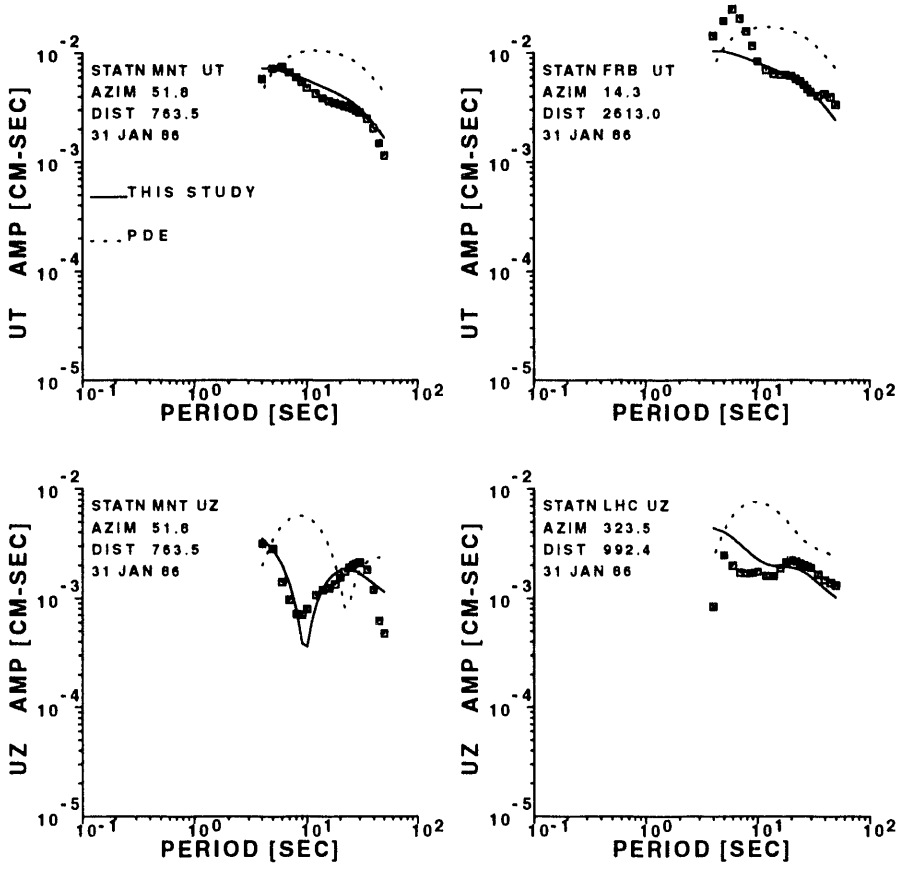

Fig. 15. Predicted (solid and dashed lines) and observed (squares) spectral amplitudes for some selected stations (UZ=Rayleigh waves, UT=Love waves) of the Perry, Ohio mainshock 31 January 1986. Eigenfunctions were computed from the crustal model obtained by inversion (Table 6, Columns 1 and 4; Figure 17). Source parameters are from this study and from Harvard CMT (PDE).

spectral amplitudes using the Harvard CMT (PDE) solution are too high, indicating a mis-estimate of seismic moment and mechanism. The predicted spectral hole in the MNT UZ spectra toward longer periods with respect to the observed data, indicating that the Harvard CMT source depth of 15 km is too deep.

DISCUSSION

In this paper, we presented a search technique for source parameter estimation. The technique was used to study eight earthquakes which occurred in central and eastern North America in recent years. The results were previously reported in theses (Nguyen, 1985, 1988) or technical reports (Herrmann and Nguyen, 1988). Since the technique relies on absolute spectral amplitudes, the phases, and hence, phase velocities are not directly fit or known. The assumption is that the eigenfunctions calculated from those crustal

models that satisfy group velocity information would be sufficient for source retrieval even though the phase velocity may not be fit as well. Since phases and phase velocities are not factors in the analysis, the shape of the absolute values of modal spectral amplitudes provides information on the focal mechanism (e.g., dip, slip, and strike); the level of the modal spectral amplitudes provides the seismic moment of the source and its focal depth. With a suitable frequency range and increasing station coverage, the source parameter becomes better constrained.

These earthquake source parameters obtained by surface waves and constrained by P-wave first motions indicate that near horizontal pressure axes (P) were in the direction of ENE-WSW compression for the Miramichi, New Brunswick (Canada), the Gaza, New Hampshire, the Arkansas, and Goodnow, New York earthquakes. The near horizontal tension axis (T) is in the NNE-SSW extension for the Wyoming earthquake. The solutions obtained are consistent with the regional stress patterns of Zoback and Zoback (1980). We summarize our focal mechanism results for the eight earthquakes studied in Figure 16 and Table 5.

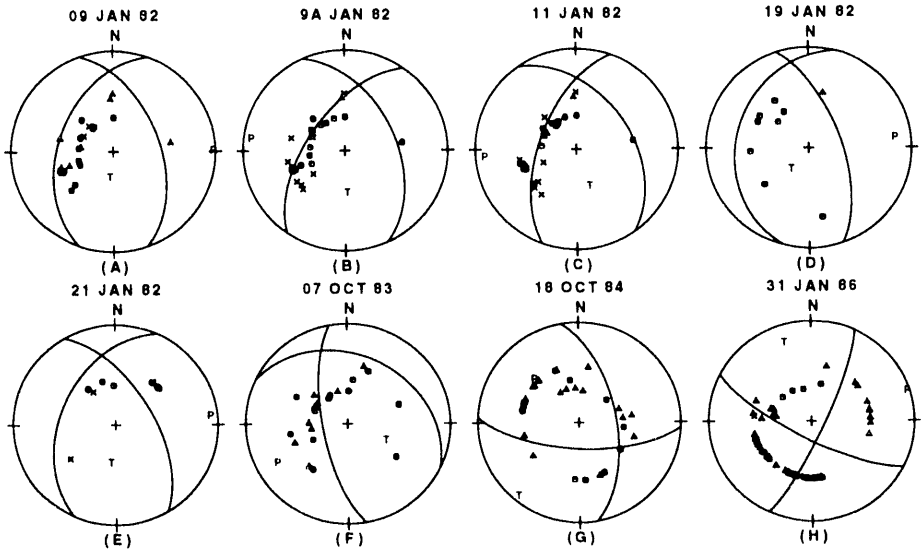

Fig. 16. Summary of focal mechanisms for the eight earthquakes studied (Table 5).

Out of the eight earthquakes analyzed, six were of predominant reverse dip slip motions (the 1982 Miramichi, New Brunswick mainshock and two large aftershocks, the 1982 Gaza, New Hampshire mainshock, the 1982 Arkansas mainshock, and the 1983 Goodnow, New York mainshock) and two were of predominant strike-slip motions (the 1984 Wyoming and the 1986 Perry, Ohio). While the depths of seven events were within the upper 10 km, the Wyoming event was deeper at 25 km.

The P-wave first-motion readings, while providing the nodal-plane constraint to surface-wave focal mechanisms, are best when read at shorter distances, when the P-wave signal-to-noise ratio is high and when there are numerous stations. The best examples are for the P-wave first motions used after the relocation of the Gaza, New Hampshire main event and those for the Perry, Ohio main event. The first motions for the Gaza, New Hampshire event were read from many available network stations with distances on the order of a few hundred kilometers from the source. The relocation of the Gaza, New Hampshire event with better P-wave arrival times helps indicate a clear agreement with the dip-slip motion obtained by surface waves from this study or with the dip-slip fault plane solution obtained by Ebel and Bouck (1988) rather than with the strike slip solution reported in Pulli *et al.* (1983) or in Sauber (1985).

On the other hand, the first motions at longer distances and/or the lack of network stations make the readings difficult to ascertain. The example is the readings for the Wyoming event. The P-wave first motions obtained for the Wyoming event only gave fair agreement to our surface-wave focal mechanism and to the mechanism by Gordon and Needham (via Langer, 1985). They do not fit our preferred solution as well as the mechanism given by the Harvard CMT (PDE). Overall, the less than perfect agreement between P-wave first motions and surface-wave focal mechanism is due to the use of various earth models for defining the P-wave take-off angles, based on the Herrin *et al.,* (1968) P-tables for teleseismic distances and simple flat-layered velocity models for regional distances.

The long period surface-wave data provided a strong constraint on source depth, which served to complement existing regional network data, which often cannot resolve depth well. In addition, the strong constraint on focal mechanism nodal planes assisted in the determination of the focal mechanism using regional network data.

CRUSTAL STRUCTURES

Table 6 and Figure 17 give for the crustal structures obtained by joint inversion of average first-higher mode and fundamental-mode group velocities of Love and Rayleigh waves after the MFT and FVF operations. Also included in this table is the central U.S. crustal model (CUS) taken from Herrmann *et al.* (1980). The P-wave velocity is derived from S velocity using a fixed Poisson's ratio of 0.25 (Bullen and Bolt, 1985). Also, density is derived from the P-wave velocity using the Nafe-Drake relation in the upper crust (Talwani *et al.,* 1959) and at depth using Birch's law (Birch, 1964). for the crustal structures obtained by joint inversion of average first-higher mode and fundamental-mode group velocities of Love and Rayleigh waves after the MFT and FVF operations. Also included in this table is the central U.S. crustal model (CUS) taken from Herrmann *et al.* (1980). The P-wave velocity is derived from S velocity using a fixed Poisson's ratio of 0.25 (Bullen and Bolt, 1985). Also, density is derived from the P-wave velocity using the Nafe-Drake

relation in the upper crust (Talwani *et al.,* 1959) and at depth using Birch's law (Birch, 1964).

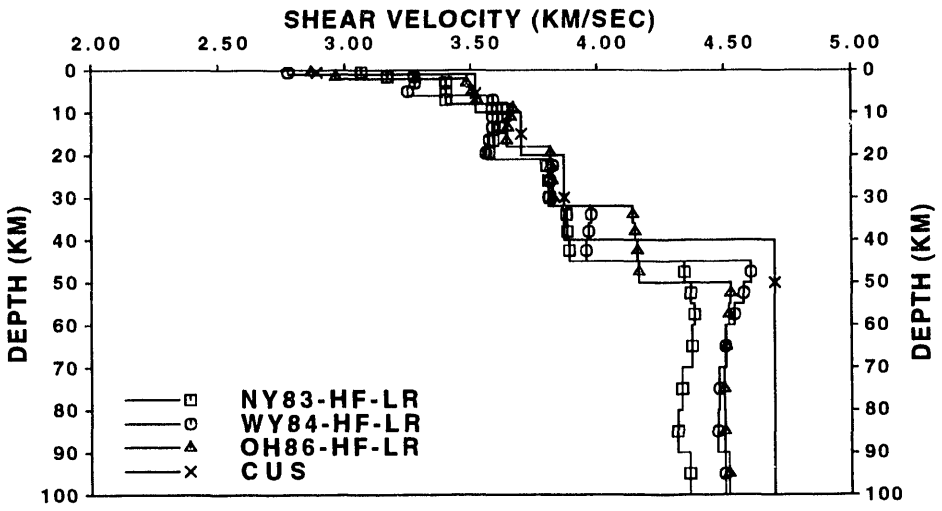

Fig. 17. Plots of crustal structures used for source studies.

Table 6
Crustal Structures Used For Surface-Wave Source Studies

	New York	Wyoming	Ohio	CUS	
H (km)	V_S (km/s)	V_S (km/s)	V_S (km/s)	H (km)	V_S (km/s)
1.00	3.07	2.77	2.87	1.00	2.89
1.00	3.17	3.28	2.96	9.00	3.52
2.00	3.40	3.28	3.48	10.00	3.70
2.00	3.40	3.25	3.51	20.00	3.87
2.00	3.40	3.59	3.53	0.00	4.70
2.00	3.63	3.59	3.67		
2.00	3.63	3.59	3.66		
3.00	3.62	3.59	3.65		
3.00	3.59	3.57	3.64		
3.00	3.57	3.56	3.81		
3.00	3.80	3.82	3.82		
4.00	3.81	3.82	3.82		
4.00	3.81	3.81	3.83		
4.00	3.88	3.98	4.14		
4.00	3.88	3.97	4.15		
5.00	3.89	3.96	4.16		
5.00	4.34	4.61	4.16		
5.00	4.37	4.58	4.52		
5.00	4.38	4.54	4.52		
10.00	4.37	4.51	4.51		
10.00	4.33	4.48	4.50		
10.00	4.32	4.47	4.50		
10.00	4.36	4.50	4.52		
0.00	4.48	4.58	4.55		

Columns 1 and 2: Shear model obtained from a joint inversion of average first higher mode and fundamental mode Love and Rayleigh wave group velocity data of the Goodnow, New York earthquake (NY83-HF-LR in Figure 17).

Columns 1 and 3: Shear model obtained from a joint inversion of average first higher mode and fundamental mode Love and Rayleigh wave group velocity data of the Wyoming earthquake (WY84-HF-LR in Figure 17).

Columns 1 and 4: Shear model obtained from a joint inversion of average first higher mode and fundamental mode Love and Rayleigh wave group velocity data of the Perry, Ohio earthquake (OH86-HF-LR in Figure 17).

Columns 5 and 6: Shear model of the central United States (CUS) (Herrmann *et al.*, 1980).

BROADBAND SEISMOLOGY AND REGIONAL SEISMIC NETWORKS

R. B. Herrmann

INTRODUCTION

The New Madrid Seismic Zone includes the locations of three very large earthquakes ($m_b > 7.0$) during the winter of 1811-1812. Most of the larger earthquakes, $m_b > 5.2$, in the central United States since then have occurred in this zone (Mitchell *et al.*, 1991). Focal mechanisms have been obtained for a number of the modern earthquakes. When combined with other crustal stress data, earthquake focal mechanisms in the region are consistent with E-W or ENE-WSW orientations of maximum compressive stress (Zoback and Zoback, 1991; Zoback, 1992). Some previously inconsistent focal mechanisms were revised (c.f. next section of this report) and are now consistent with this overall trend. Given this agreement, the thrust of focal studies now is on the relation of nodal planes to spatial seismicity patterns and on the dependence of strong ground motion on the particular mechanism.

Regional seismic activity has been monitored by a variety of seismographs since the installation of the 80 kg Wiechert at Saint Louis University in 1909. Significant milestones in instrumentation were the installations of WWSSN long period instrument in the 1960's, the regional seismic network in 1975 and the broadband digital IRIS station at CCM in 1989, and the local deployment of the dense PANDA array in 1989-1992 (Y. T. Yang, Memphis State University 1993, personal communication).

The object of this paper is to derive source parameters for two large earthquakes that occurred in the zone during 1990-1991, and to assess how regional network data can complement broadband digital data. The two earthquakes are those of September 26, 1990 and May 4, 1991. The origin time and location of these events are given in Table 7. Figure 18 shows the location of these two events with respect to the regional network seismicity. In addition, the location of the IRIS station CCM is indicated. It is seen that the May 4, 1991 earthquake is near the dense linear seismicity patterns new New Madrid, while the September 26, 1990 earthquake is on the periphery of the very active zone. The seismograph station distribution of the regional network roughly parallels the density of the seismicity.

EARTHQUAKE OF SEPTEMBER 26, 1990

This earthquake is interesting for a number of reasons. First its location is along a diffuse northwest seismicity trend to the north of the strong linear seismicity trends of the central portion of the New Madrid Seismic Zone (Figure 18). In addition, the $m_{Lg} = 4.5$ earthquake occurred at the edge of the regional seismic network. The nearest seismograph station was 31 km away, and thus has poor depth control which depends upon sensitivity to first

Table 7
Event Information for Waveform Studies

Date	Origin Time (UT)	Lat (°N)	Lon (°W)	Depth (km)	Strike (°)	Dip (°)	Rake (°)	Moment (dyne-cm)
092690	1318	37.16	89.58	15	140	75	50	3.0E+22
050491	0118	36.56	89.83	8	90	67.5	20	1.8E+22

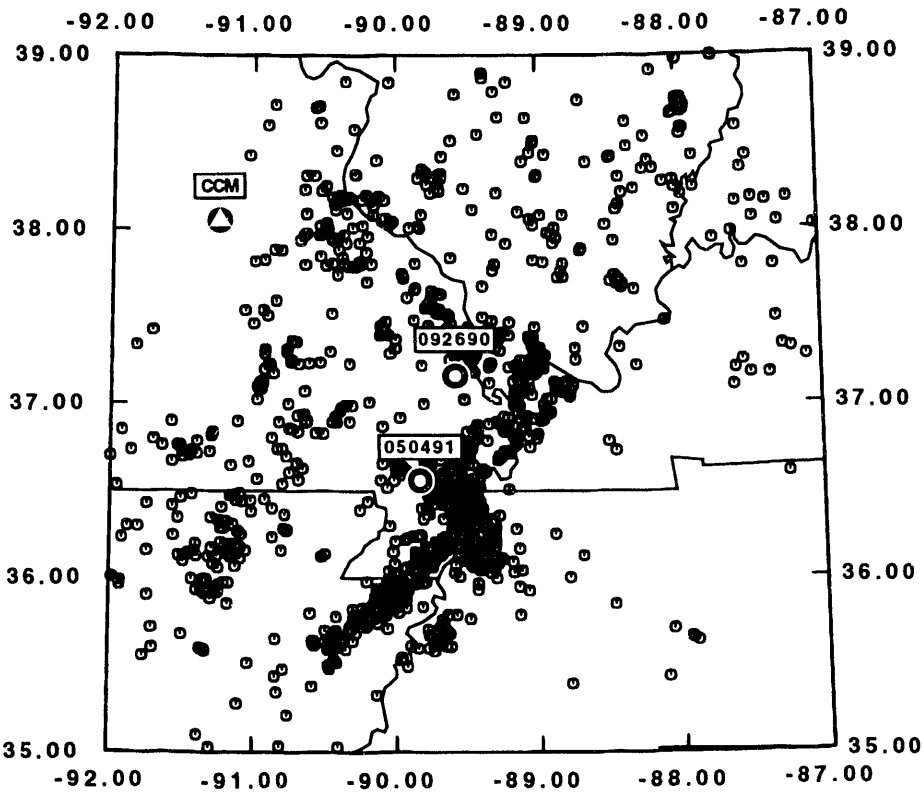

Fig. 18. Location of the September 26, 1990 and May 4, 1991 earthquakes in the New Madrid Seismic Zone in relation to the seismicity contained in the regional seismic network catalog from 1975 - 1992. The location of the IRIS station CCM is also indicated.

arrival cross over distances in the crustal model used rather than to the curvature of the travel time curve and good S-P arrival time differences at short distances. Finally, because of the lack of seismograph stations directly above the source, the focal sphere coverage of P-wave first motion data is not sufficient to completely define the nodal planes of the focal mechanism.

The broadband signal at CCM, a distance of 175 km at an azimuth of 305°, was passed through a WWSSN 15-100 instrument response with a peak gain of 1.0. These observed three component seismograms are shown as the upper traces in Figure 19. Shown in the upper right

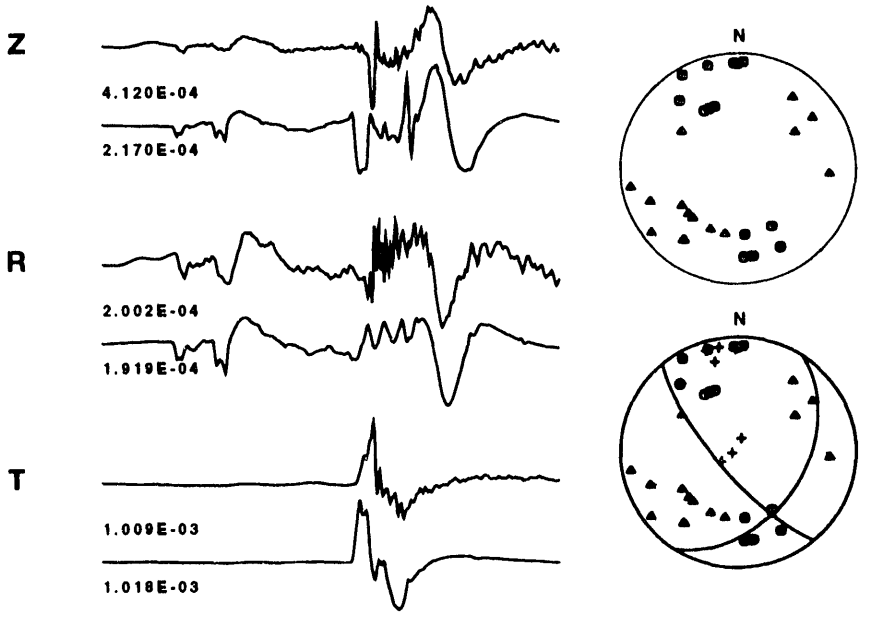

Fig. 19. Comparison of observed and synthetic (upper and lower traces, respectively, for each component) time histories for the September 26, 1990 earthquake recorded at the IRIS station CCM. Both sets are passed through a 15-100 WWSSN LP instrument response with a peak gain of 1. A total of 51.1 seconds of time history is displayed, starting 20 seconds after the event origin time. The lower hemisphere equal area projections to the right show the observed P-wave first motion data from the main event (upper), and the main and aftershock first motion data (lower). The mechanism plotted is that required by the waveform fit. A circle or plus sign indicates a compression, and a triangle or minus sign indicates a dilatation. Positive Z, R and T values represent motion up, away from the source, and in a direction clockwise about the source.

hand corner of this figure, are the observed P-wave first motion data for the earthquake plotted in a lower hemisphere equal-area projection. As can be seen, a number of focal mechanisms can be placed through these observations, depending on the number of inconsistencies permitted.

To use the broadband signal to constrain the focal mechanism, synthetic seismograms were generated using the CUS model of Table 8. This model is derived from the simple crustal model given by Nuttli *et al* (1969) and was used by Herrmann (1979c) in synthetic seismogram modeling. The model does a reasonable job in explaining surface-wave group velocity dispersion in the 5 - 50 second period range in the mid-continent. Wavenumber integration code was used to generate synthetics. Rather than attempt a true waveform inversion, synthetics were generates for a suite of strike, dip and rake values for a double couple source at different depths. The choice of the strike, dip

Table 8
Earth Models Used for Synthetics

H (km)	V_P (km/sec)	V_S (km/sec)	ρ (gm/cm^3)	Q_P^{-1}	Q_S^{-1}
CUS					
1.00	5.0	2.89	2.5	.005	.01
9.00	6.1	3.52	2.7	.0005	.001
10.00	6.4	3.70	2.9	.0005	.001
20.00	6.7	3.87	3.0	.0005	.001
	8.15	4.70	3.4	.0005	.001
MALDEN					
1.00	4.89	2.83	2.5	.005	.01
9.00	5.98	3.44	2.7	.0005	.001
10.00	6.21	3.59	2.8	.0005	.001
10.00	6.44	3.72	2.8	.0005	.001
10.00	6.47	3.74	2.8	.0005	.001
20.00	7.97	4.60	3.3	.0005	.001
	8.05	4.65	3.3	.0005	.001
HELM					
5.50	5.5	3.00	2.4	.0005	.001
9.50	6.3	3.60	2.6	.0005	.001
19.00	6.7	3.80	2.8	.0005	.001
	7.8	4.30	3.32	.0005	.001
JD					
2.00	5.1	3.02	2.5	.0005	.001
6.00	5.8	3.45	2.65	.0005	.001
14.00	6.2	3.65	2.73	.0005	.001
14.00	6.9	3.85	2.90	.0005	.001
	7.9	4.40	3.21	.0005	.001
KH					
4.00	5.5	3.18	2.4	.0005	.001
22.00	6.3	3.60	2.6	.0005	.001
6.00	6.8	3.90	2.8	.0005	.001
	7.8	4.50	3.3	.0005	.001
SC					
5.50	5.5	3.18	2.4	.0005	.001
10.50	6.3	3.64	2.67	.0005	.001
19.00	6.6	3.87	2.8	.0005	.001
	7.8	4.50	3.1	.0005	.001
SD					
5.50	5.5	3.10	2.4	.0005	.001
10.50	6.3	3.55	2.67	.0005	.001
19.00	6.6	3.87	2.8	.0005	.001
	7.8	4.55	3.1	.0005	.001

Models HELM, JD, KH, SC and SD are from L.S. Zhao and D. V. Helmberger (1993, California Institute of Technology, personal communication).

and rake angles was based on visual examination of P-wave first motion data

in Figure 18.

Synthetics were then visually compared to the observed signal. A goodness of fit criteria was based on several observations in the observed signals. First, the P-wave first motion is a dilatation. Second, the phase approximately 5 seconds after *P* (identified as *sP* by C.A. Langston, 1993, Pennsylvania State University, personal communication) is also a dilatation. Third, the first motion on the tangential component is positive. Fourth, the ratio of peak amplitudes on the Z, R, and T components is roughly 1, 1, and 5, respectively (ignoring the high frequency spike on the Z component). Finally, the shape of the Rayleigh wave pulse on the Z and R components is used. Even though this qualitative set of criteria is hard to quantify, the final solution was very sensitive to changes in strike, dip and rake angles of 10°.

The waveforms do not uniquely define the focal mechanism. One solution had a strike of 320°, a dip of 70° and a rake of 40° but had 12 P-wave first motion inconsistencies. The Z and R synthetics were in excellent agreement, but the predicted *SH* arrival on the T component was more complex than observed. The solution finally accepted is listed in Table 7 and plotted in Figure 19. This solution has only four inconsistencies. It is also consistent with aftershock data indicated by the + signs in the focal mechanism displayed at the lower right in Figure 19 (of course this assumes that the aftershocks and the main event have the same focal mechanisms).

The other aspect is that the focal depth was shown to be 15 km rather than 10 or 20 km. This is consistent with focal depths of 10 - 16 km for aftershocks located using regional network data as well as readings from portable instruments deployed above the hypocenter (Taylor and Wuenscher, 1990).

To appreciate the sensitivity of the seismogram to source depth, Figure 20 compares synthetics for the same focal mechanism and seismic moment but for source depths of 5, 10, 15 and 20 km in the CUS model. The effect of focal depth is seen in a number of ways. First, the Rayleigh-wave pulse on the Z and R traces broadens as depth increases. Second, the separation between *P* and *sP* increases with depth. Finally, the high frequency spike following *S* on the vertical component is very depth dependent, but is not observed well enough in the observed data to use. The *sP* arrival is very prominent for this event because of its depth and focal mechanism.

L.S. Zhao and D. V. Helmberger (1993, California Institute of Technology, personal communication) describe a procedure for rapid source parameter estimation from broadband data by using imperfect Green's functions. The method consists of windowing the seismogram to focus on the P-wave arrival and the surface-wave arrivals separately. The inverse is based on the best fit to these phases and is not overly sensitive to the particular earth model because of the windowing procedure. That paper discusses four different earth models for paths in southern California. Since these models are being considered for waveform modeling, it is appropriate to see how well they do in fitting the waveform of the September 26, 1990 earthquake. This would

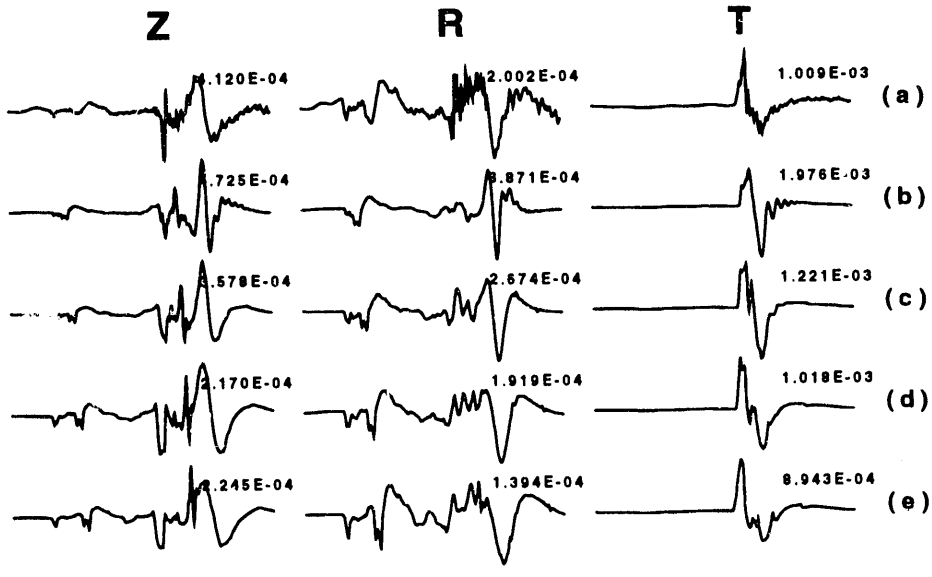

Fig. 20. Comparison of observed WWSSN 15-100 response to synthetics for different source depths in CUS earth model for the September 26, 1990 earthquake. (a) Observed time history; (b) 5 km; (c) 10 km; (d) 15 km; (e) 20 km. All time histories are 51.1 seconds long and start 20 seconds after origin time.

provide a test of the sensitivity of waveform inversion scheme to an exact earth model.

Figure 21 presents synthetic seismograms to compare with the CCM observations. The source parameters used are those given in Table 7 for this earthquake. The models are given in Table 8. It is obvious that the *P* and *sP* arrivals are not very sensitive to the earth model, either in amplitude or arrival time difference. The pulse width of the Rayleigh wave is similar, even though differences in upper crustal shear-wave velocity gives them different phase angles. The major difference between the models is in the arrival time and sharpness of arrivals following S on the Z component and in the nature of the S-wave arrivals on the T component. The apparent particle motion of the sharp arrivals on the vertical component indicate that these arrivals are due to some conversion of *S* to *P* on its final leg. The conclusion is that focal mechanism estimates of these low frequency waveforms may not be overly sensitive to the velocity model used and also that the waveforms contain significant information about structure.

EARTHQUAKE OF MAY 4, 1991

This earthquake occurred near the towns of Risco and Malden, Missouri. This event occurred well within the station distribution of the New Madrid Regional Seismic Network but also within the dense PANDA deployment (Y. T. Yang, Memphis State University, 1993, personal communication). Because

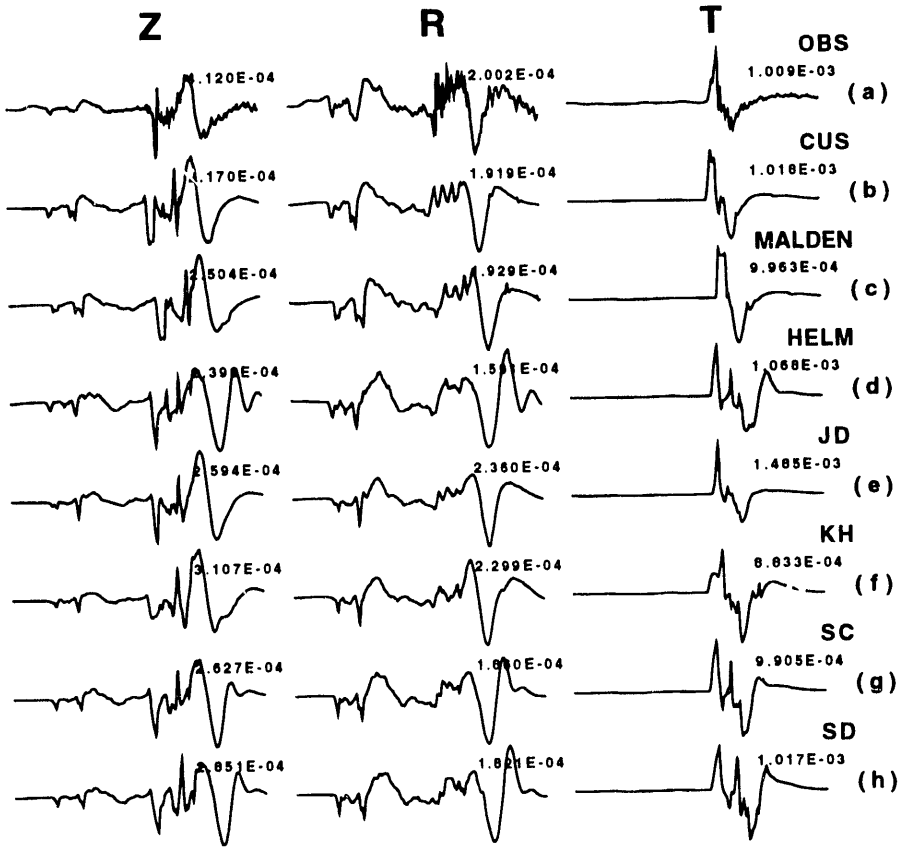

Fig. 21. Test of sensitivity to earth model for September 26, 1990 earthquake. (a) observed All times histories are for a WWSSN 15-100 long period response, start 20 seconds after the origin time, and continue for 51.1 seconds. The synthetics are generated using the source parameters of Table 7. (a) observed time history; (b) CUS model; (c) MALDEN model; (d) HELM model; (e) JD model; (f) KH model; (g) SC model; (h) SD model.

of this location relative to the two seismic networks, the focal depth of the event is well defined and is given as 6.9 km by these authors. In addition, the focal mechanism is relatively well constrained.

Figure 22 presents the observed P-wave first motion data, the observed seismograms and the synthetic seismograms that fit the data well. The dip of the east-west nodal plane of Figure 22 is not well constrained from the first-motion data and can vary in dip from south to north. The waveform data do require the dip to the south by the amount shown.

Several observations can be made by comparing the seismograms. First the depth is shallow because of the short separation between *P* and *sP*. Second, the Rayleigh and SH arrivals are predicted too early. Finally, the shape of the Rayleigh pulse on the Z component is slightly out of phase.

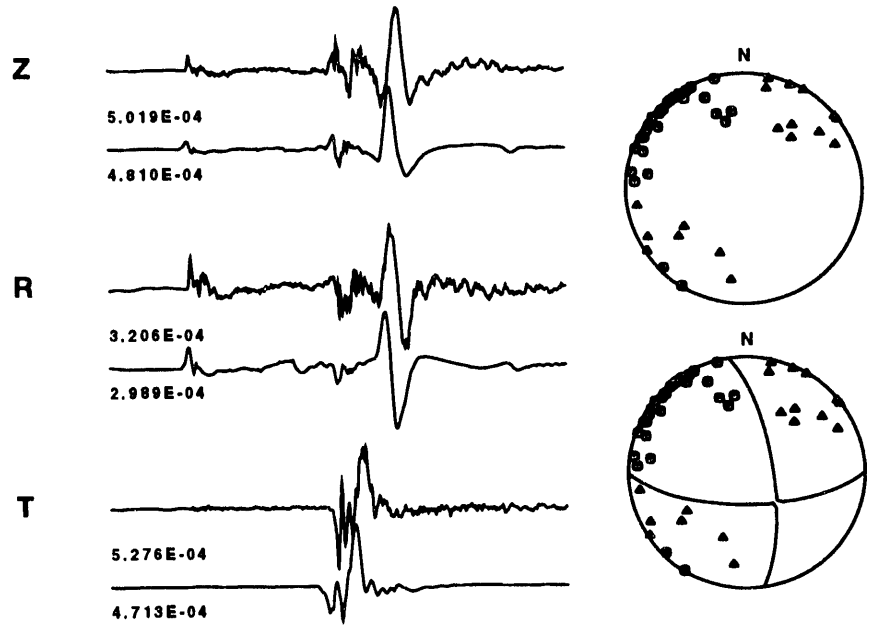

Fig. 22. Comparison of observed and synthetic (upper and lower traces, respectively, for each component) time histories for the May 4, 1991 earthquake recorded at the IRIS station CCM. Both sets are passed through a 15-100 WWSSN LP instrument response with a peak gain of 1. A total of 80 seconds of time history is displayed, starting 20 seconds after the event origin time. The lower hemisphere equal area projections to the right show the observed P-wave first motion data from the event with (upper) and without (lower) the focal mechanism superimposed. Circles and triangles indicate compressional or dilatational P-wave first-motion, respectively. The CUS model is used.

Figure 23 shows the sensitivity of the synthetics to focal depth, which is permitted to vary from 5 to 20 km. The *sP* phase is not very prominent as a depth indicator, but the duration of the Rayleigh-wave pulse is seen to be a function of focal depth. The 8 km depth chosen for this earthquake is seen to provide a reasonable agreement in the duration of the Rayleigh wave.

To reconcile the problems with the Rayleigh- and SH-wave arrival times, the arrivals were modeled as a single mode surface wave, and the phase difference in the complex signal was used to define an improved phase velocity dispersion between the source and receiver, and thus a better earth model (last section). The result is the MALDEN model of Table 8. The big difference between this model and the CUS models, is that the shear-wave velocity is lower throughout the entire crust by about 0.1 km/s or about 3% (Langston, 1993, Pennsylvania State University, personal communication, also noted the need for a slower model). The synthetics for this model are shown in Figure 24. Note the better agreement in the arrival time of the large positive amplitudes on the three components, as well as the phase of the Rayleigh wave pulse on the Z component. Figure 25 studies the sensitivity of the synthetics

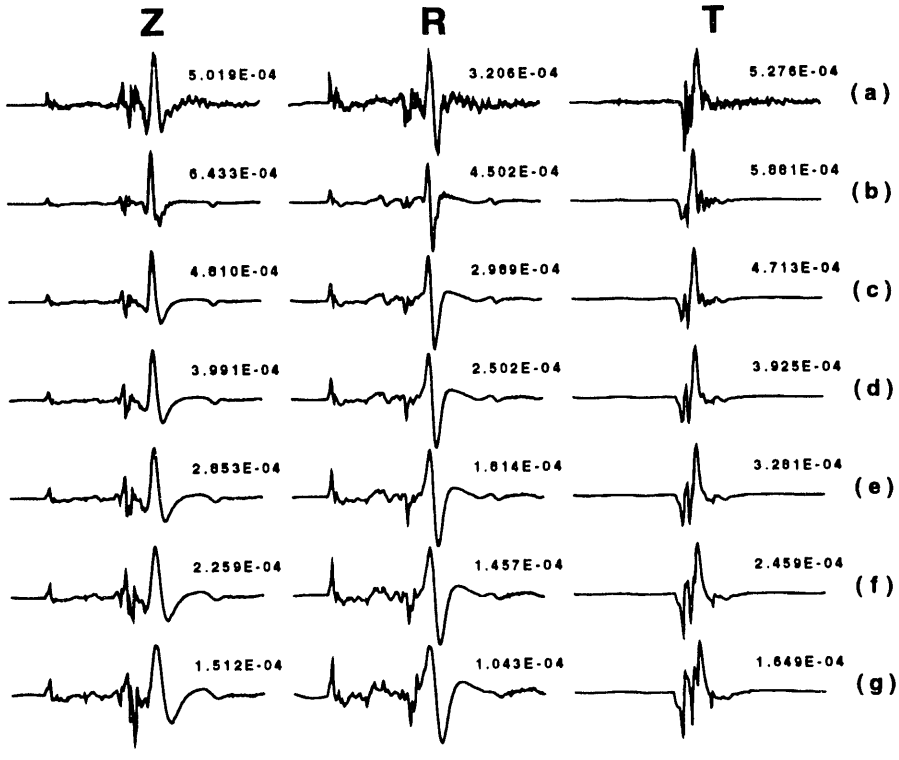

Fig 23. Comparison of observed WWSSN 15-100 response to synthetics for different source depths in CUS earth model for the May 4, 1991 earthquake. (a) Observed time history; (b) 5 km; (c) 8 km; (d) 10 km; (e) 12 km; (f) 15 km; (g) 20 km. All time histories are 81.2 seconds long and start 20 seconds after origin time.

to focal depth for this model, again showing that the Rayleigh wave pulse width demands a shallow source.

DISCUSSION

The focal mechanisms obtained here are similar to those found in Langston (1993, Pennsylvania State University, personal communication), but differ somewhat because of the nature of his shear-wave velocities in the lower crust. This study was not a direct attempt at waveform inversion, but rather an exploratory study to test the feasibility of such an inversion. Regional seismic network data were necessary to provide a first order constraint on the focal mechanism through the P-wave first motion data and through the depth estimate, even though the waveforms are capable of defining depth.

To see how these focal mechanisms agree with other solutions, they are plotted together with the seismicity in Figure 26. The other focal mechanisms, including corrected mechanisms for the July 21, 1967 earthquake at the upper left corner of the figure, and the March 3, 1963 earthquake just west of the May 4, 1991 earthquake are taken from the next section. The May 4,

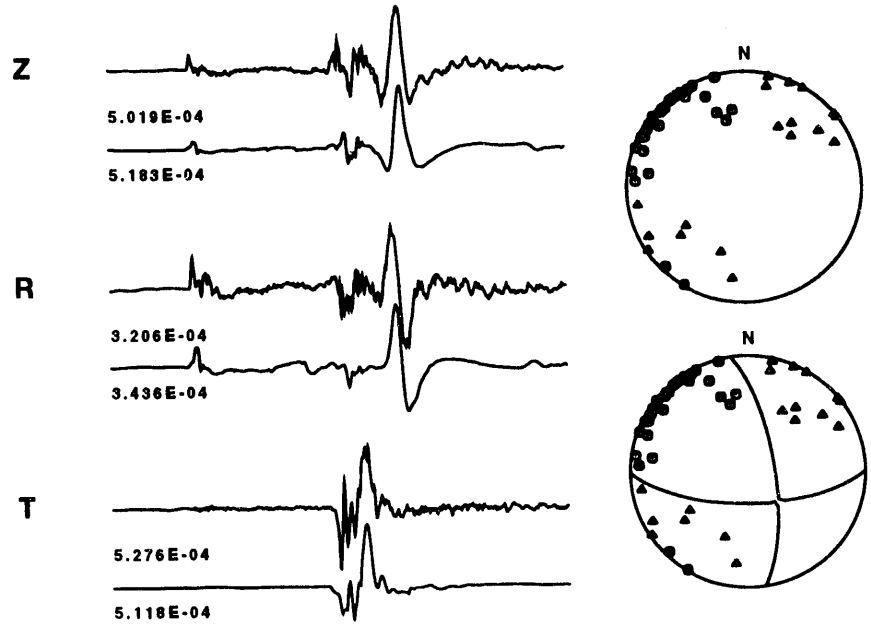

Fig. 24. Comparison of observed and synthetic (upper and lower traces, respectively, for each component) time histories for the May 4, 1991 earthquake recorded at the IRIS station CCM. Both sets are passed through a 15-100 WWSSN LP instrument response with a peak gain of 1. The first motion information is described in Figure 22. The MALDEN model is used. Note the better agreement in arrival time and phase of the surface waves.

1991 earthquake lies an east-west seismicity trend, and on the basis of this, the east-west striking nodal plane can be assumed to be the fault plane. The September 26, 1990 earthquake is plotted at the top center of the figure. There is only a diffuse pattern of seismicity for it to be associated with. However, the east-west trending P-axis is consistent with the other mechanisms in the area and also with compressive stress patterns in the mid-continent (Zoback and Zoback, 1991; Zoback, 1992).

An interesting feature of the study is the sensitivity of the long period portion of broadband data to earth structure. The CUS model was adequate for describing the gross features of the observed waveform of the September 26, 1990 earthquake. However, it was not able to describe the high frequency arrival following *S* on the R component and especially the large amplitude *S* pulse on the Z component. To illustrate this Figure 27 compares the observed and synthesized ground velocities after being low pass filtered with different corner frequencies. The source parameters of Table 7 were used together with the CUS earth model of Table 8. As higher frequencies are introduced by increasing the corner frequency, the agreement between the observed and synthetics decreases in terms of shape, frequency content and peak amplitude. This is not unexpected since the earth model used is a very simple

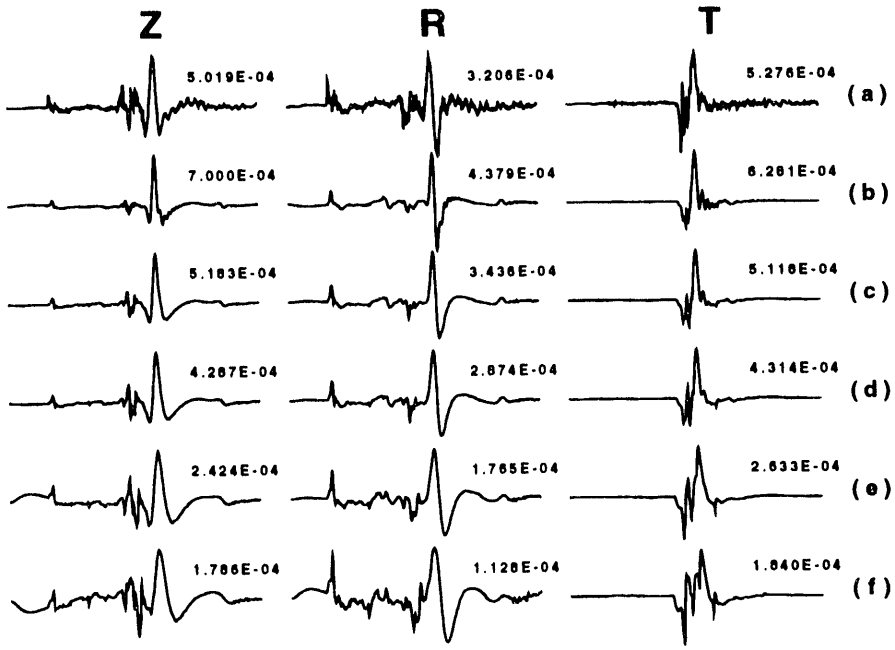

Fig 25. Comparison of observed WWSSN 15-100 response to synthetics for different source depths in MALDEN earth model for the May 4, 1991 earthquake. (a) Observed time history; (b) 5 km; (c) 8 km; (d) 10 km; (e) 15 km; (f) 20 km. All time histories are 81.2 seconds long and start 20 seconds after origin time.

plane layered structure. Adding more detail to the model may improve the fit. The problem of an appropriate velocity model is interesting. This paper has show evidence that the earth models for earthquakes, separated by only 70 km, to the same seismograph station can differ by 2 - 4% (comparison of CUS and MALDEN models in Table 8), and that this can be resolved in modern broadband regional network seismograms. This difference in structure along two neighboring paths is not unexpected given the May 4, 1991 earthquake occurred near the edge of the Reelfoot graben and intrusive plutons (Hildenbrand, *et al.*, 1992). In the future data from additional stations will make it possible to determine whether this velocity change is uniform over the entire path or it is spatially variable. Information on the lateral variation of the crustal velocity model may provide crucial information of the reason for earthquakes in the region. Finally, the difference in high frequency waveform detail indicates the need to refine the models in order to improve predictions of high frequency ground motion for hazard mitigation.

CROSS CORRELATION FOR PHASE VELOCITY

Given a known seismic source defined in terms of its moment tensor and distribution of point forces, synthetic seismograms can easily be generated for plane layered isotropic media. If the observed signal and the synthetic consist

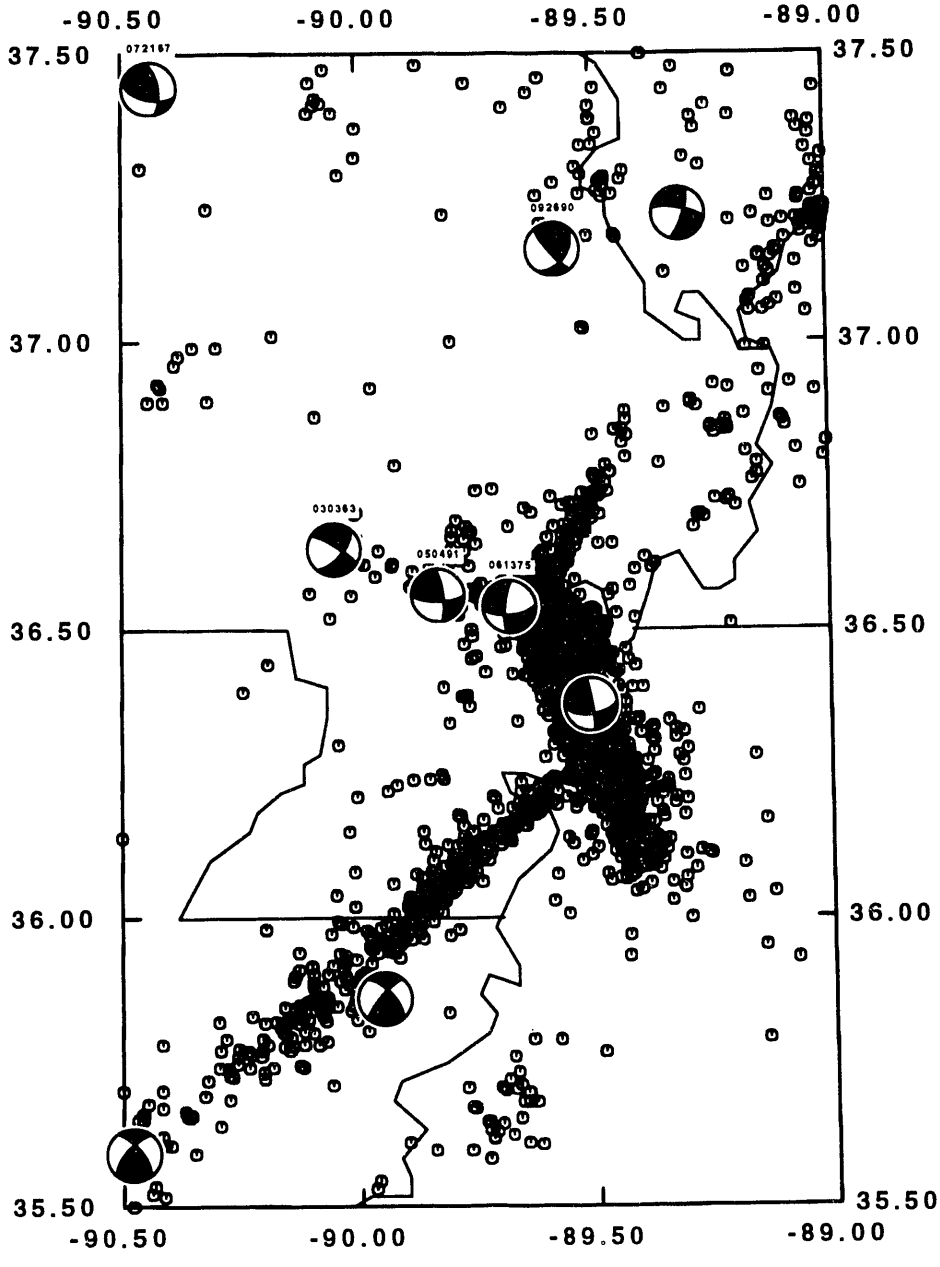

Fig. 26. Surface-wave focal mechanisms from this study in the New Madrid region superimposed on regional seismic network epicenters.

of a well defined fundamental mode surface wave, then the difference in the complex phase of the signals can be used to define the phase velocity of the observed surface wave, which in turn can be inverted for an improved velocity model. This section describes a cross correlation technique to estimate the phase velocity and, more importantly, a qualitative estimate of the confidence

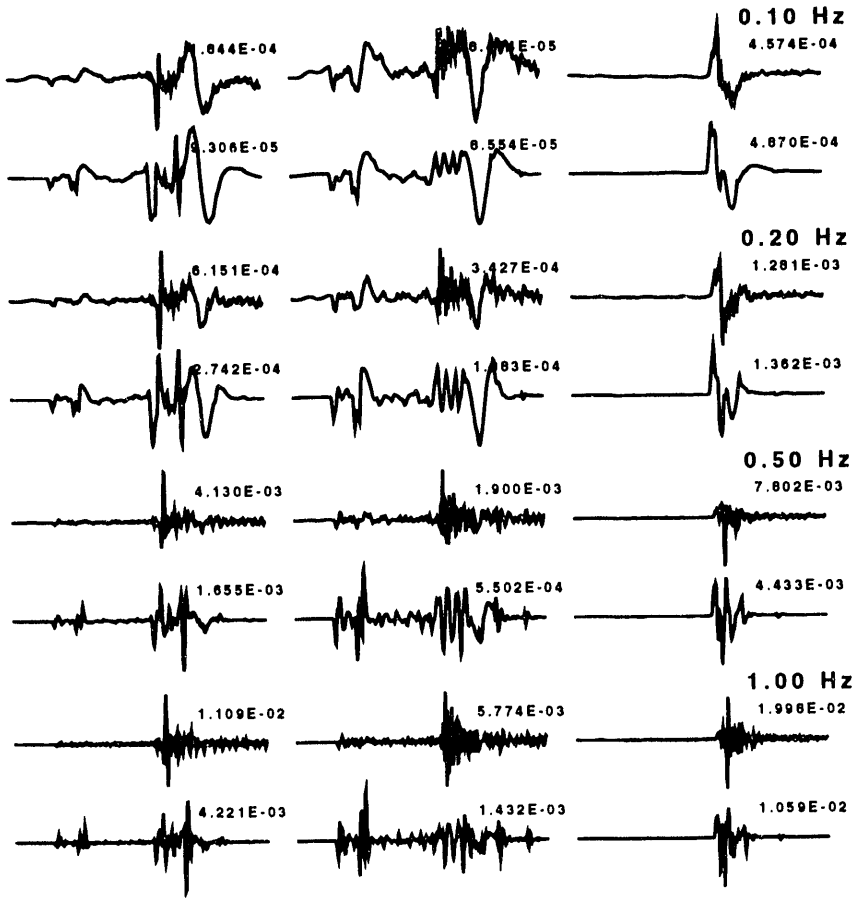

Fig. 27. Comparison of observed and CUS model synthetic time histories for the September 26, 1990 earthquake in different filter bands. The broadband velocity time histories are low pass filtered at 0.10, 0.20, 0.50 and 1.0 Hz with a second order Butterworth filter. The peak ground velocity in units of cm/s are indicated.

in the dispersion.

For simplicity let the synthetic fundamental mode signal have a Fourier transform $X(f)$ expressed as

$$X(f) = A(f)e^{i\phi(f)}e^{-ik(f)r}$$

where r is the source-receiver distance, $A(f)$ and ϕ includes the effect of source time function and surface-wave excitation, and $k(f)$ is related to the phase velocity, $c(f)$, by $k(f)=2\pi f / c(f)$.

Let the observed signal be given by

$$Y(f) = A_o(f)e^{i\psi(f)}.$$

If the observed signal only contains the fundamental mode surface wave, which is possible through appropriate time domain windowing or phase

match filtering, then

$$Y(f) = A_o(f)e^{i\Phi(f)}e^{-iK(f)r} .$$

If it is assumed that the source is known, e.g., $\Phi = \phi$, then the simple mathematical technique of cross-correlation can be used to defined the difference in phase,

$$\frac{Y(f)X^*(f)}{X(f)X^*(f)} = \frac{A(f)}{A(f)} e^{-i(K(f)-k(f))r}$$

where the * symbol represents a complex conjugate. The phase of the left hand side can be interpreted in terms of the difference in wavenumber, and effectively the phase velocity, between the observed and synthetic.

If the assumptions of knowing the source phase and having only a single mode in the observed signal are not met, then the inferred phase velocity correction cannot be accepted with confidence. This difficulty can be addressed by using smoothed spectra and a statistical test (Jenkins and Watts, 1968; Shumway, 1988).

The time series $x(t)$ and $y(t)$ are windowed between $t_{\min}$ and $t_{\max}$ to provide windowed complex Fourier spectra $X(f)$ and $Y(f)$. From these two spectra the the autocorrelation and cross correlation spectra are defined from the relations

$$XY(f) = Y(f)X^*(f)$$

$$XX(f) = X(f)X^*(f)$$

$$XY(f) = Y(f)X^*(f)$$

The smoothed spectra $\overline{XY}$, $\overline{XX}$ and $\overline{YY}$, at a frequency $f = k\Delta f$ are computed from formulas of the form

$$\overline{XY}(k) = \frac{1}{L} \sum_{n=-(L-1)/2}^{(L-1)/2} XY(k+n),$$

the coherency squared, κ_{12}^2, from

$$\kappa_{12}^2 = |\overline{XY}|^2 / (\overline{XX}\,\overline{YY}),$$

and the estimated cross spectra from

$$\bar{H}(f) = \bar{A}(f)e^{i\bar{\phi}(f)} = \overline{XY}(f) / \overline{XX}(f).$$

Because of the smoothing, there is redundant information that can be used to estimate the confidence on the cross spectra. The statistical test is whether the two spectra are significantly different. Defining a factor

$$\Phi = \left(\frac{2}{2(L-1)} f_{2,2(L-1)}(1-\alpha)(1-\kappa_{12}^2)/\kappa_{12}^2 \right)^{1/2},$$

then the $100(1-\alpha)\%$ confidence bands on the amplitude and phase spectrum of the cross spectrum are

$$\bar{A}(f)(1 \pm \Phi)$$

$$\bar{\phi}(f) \pm \sin^{-1}(\Phi)$$

To estimate the phase velocity and error, let r be the distance between the two surface-wave observations and let the theoretical phase velocity used to generate the synthetic be c_m. The difference in the phase will be explained by a difference in phase velocities. The corrected phase velocity estimate is obtained from

$$\frac{1}{c} = \frac{1}{c_m} - \frac{\bar{\phi}(f)}{\omega r}$$

and the error in the phase velocity is estimated to be

$$\Delta c = c^2 \sin^{-1}(\Phi)/\omega r$$

Experimentation shows that increasing the smoothing window will reduce the coherency, and hence increase the 95% confidence limits on the phase velocity. A value of $L = 3$ is adequate. In addition, a larger L will lead to rippling in the phase velocity at high frequencies, which may be due to the use of an essentially rectangular smoothing function.

This technique was applied to the observed vertical, Z, and tangential, T, traces for the May 4, 1991 earthquake. Figure 28 shows the windowed WWSSN 15-100 long period instrument time histories. No attempt was made to isolate the fundamental mode using phase match filters.

Consider Figure 28(a) which compares the theoretically predicted vertical component Rayleigh wave arrival for a depth of 8 km and the mechanism given in Table 7 using the CUS model of Table 8 to the observed signal at CCM. The model predicted dispersion is given by the dotted curve, while the output of the cross-correlation analysis is given by the solid curve with error bars. As is obvious from the signals, the CUS model is too fast. In addition, the phase of the Rayleigh wave pulse differs. Figure 28(c) is a similar display for the Love wave. The resulting dispersion curves were inverted by starting with the CUS model and keeping Poisson's ratio fixed. The Δc values are used as weights in the inversion. The new earth model is given as the MALDEN model in Table 8. Figures 28(b) and 28(d) show the result of further processing with this newer model for the Rayleigh and Love arrivals, respectively.

First note that the arrival times of the positive peaks now agree, and that little additional change in the dispersion is required in the 0.04 - 0.25 Hz band. The improved fit shows the benefit of the analysis.

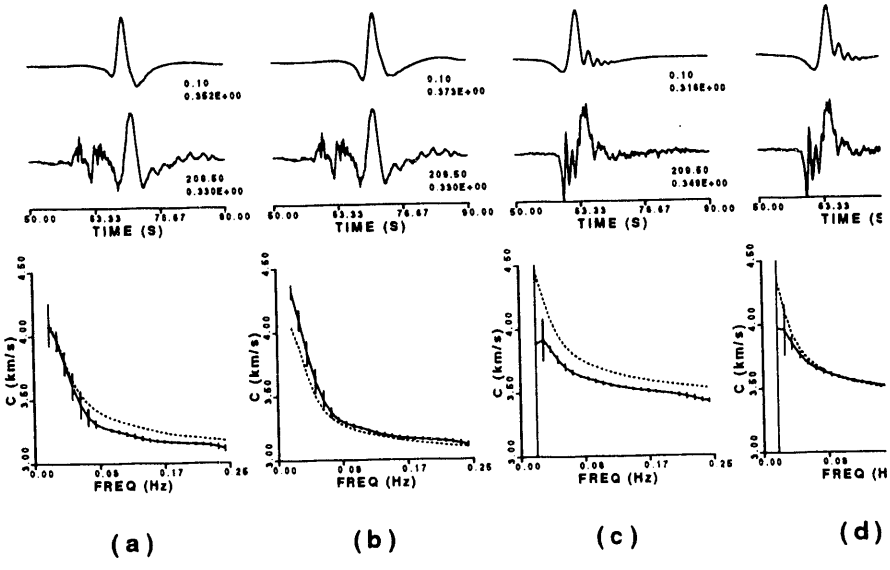

Fig. 28. Demonstration of the cross-correlation technique to revise the dispersion between the May 4, 1991 earthquake and the CCM station. (a) and (c) modification of original dispersion computed using the CUS model for the Rayleigh and Love waves, respectively. The top traces are the synthetics predicted using the CUS model. The second set of traces are the observed data. The dotted lines in the phase velocity versus frequency plot are the theoretical dispersion based on the CUS model, and the solid lines with error bars are the dispersions required to explain the signal differences. Figures (b) and (d) show the result of further processing with the Malden model of Table 1. All traces have been passed through a WWSSN 15-100 long period instrument.

BROADBAND MODELING OF REGIONAL SEISMIC EVENTS

Robert B. Herrmann

INTRODUCTION

Modeling of broadband seismograms of earthquakes at distances of up to a few hundred kilometers is proving to be a strong constraint on the focal mechanism, focal depth, seismic moment and even the source duration of these events (Dreger and Helmberger, 1991 ; Dreger and Helmberger, 1993). L. S. Zhao and D. V. Helmberger (1993, California Institute of Technology, personal communication) proposed analyzing parts of the waveform separately, to permit rapid source parameterization without being too dependent on the characterization of the true source-receiver path velocity model.

As an example of waveform modeling consider the results of analyzing two earthquakes that occurred in the New Madrid Seismic Zone in 1990 and 1991 (c.f. previous section of this report). Figure 29 shows the results for the earthquake of September 26, 1990 recorded at the IRIS broadband station CCM in Missouri. The observed and synthetic, generated using *omega – k* integration techniques, time histories are those of a 15-100 WWSSN long period instrument response with a peak magnification of 1. Trace amplitudes are given in cm units. The Z, R and T components of the time history are displayed. The seismograph station was a distance of 175 km from the event along a source-station azimuth of 305°. The location parameters of this event are given in Table 9.

This earthquake occurred on the periphery of the regional seismic networks operated by Saint Louis University and Memphis State University, and hence focal depth was poorly constrained on the basis of arrival times. In addition, the focal mechanism was also poorly constrained because of the lack of significant coverage of the focal sphere (Figure 29, upper focal sphere projection). Waveform modeling was performed by using the CUS earth model of Table 10, and by interactively displaying synthetic seismograms as the values of strike, dip, rake and source depth were changed. One good visual fit is that shown in the lower traces of Figure 29 for the mechanism listed in Table 9. This mechanism is plotted on the lower focal sphere together with additional P-wave first motion data for aftershocks obtained from the regional networks and a portable aftershock deployment (Taylor and Wuenscher, 1990). The first motion fit using the mechanism demanded by the waveform match is excellent, with only four inconsistencies, which could be related to the dependence of the takeoff angle upon the earth model used. Finally, the waveform inferred depth of 15 km is consistent with 10 - 16 km aftershock depth range constrained by readings from portable seismographs directly above the aftershocks (Taylor and Wuenscher, 1990).

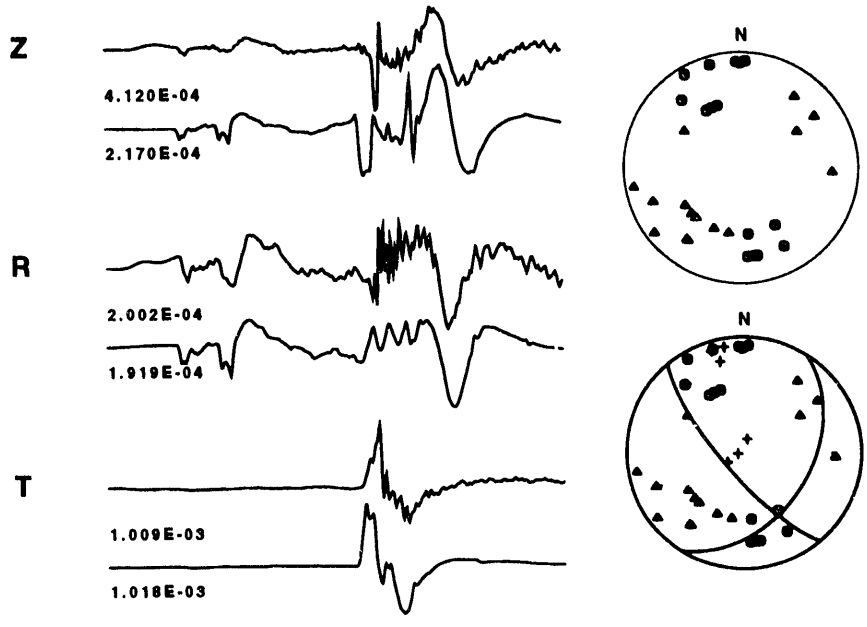

Fig. 29. Comparison of observed and synthetic (upper and lower traces, respectively, for each component) time histories for the September 26, 1990 earthquake recorded at the IRIS station CCMV. Both sets are passed through a 15-100 WWSSN LP instrument response with a peak gain of 1. A total of 51.1 seconds of time history is displayed, starting 20 seconds after the event origin time. The lower hemisphere equal area projections to the right show the observed P-wave first motion data from the main event (upper), and the main and aftershock first motion data (lower). The mechanism plotted is that required by the waveform fit. A circle or plus sign indicates a compression, and a triangle or minus sign indicates a dilatation. Positive Z, R and T values represent motion up, away from the source, and in a direction clockwise about the source.

The second earthquake studies is that of May 4, 1991, which occurred near New Madrid. Figure 30 compares the 15-100 WWSSN LP reponses of the observed and predicted time histories at CCMV. The station was a distance of 209 km along an azimuth of 323° from the event. As can be seen from the first motion data, a strike-slip solution is required, but that there considerable variation permitted in the nodal plane orientations.

Waveform modeling with the CUS model fit the data, but had the predicted surface-wave pulses arriving earlier than observed. Since this event was in the center of the regional seismic network and also within the dense Memphis State PANDA deployment, origin time and source depth were well constrained, even though the waveforms demand the same 8 km depth. In order to match the waveforms, a modified earth model, denoted by MALDEN in Table 10 was used. This model is the one used to make the synthetics. The mechanism listed in Table 9 provides an excellent fit to the observed waveform in phasing and absolute amplitude, and also fits the observed P-wave first motion data well. The few inconsistencies are expected with the quality of regional network data and sensitivity of takeoff angles to earth model.

Table 9
Comparison of Source Parameters

Date	Origin Time (UT)	Lat (°N)	Lon (°W)	Depth (km)	Strike (°)	Dip (°)	Rake (°)	Moment (dyne-cm)	Ref
Previous Results									
020262	0643	36.37	89.51	7.5	350	84	145	2.5E+22	(1,2)
030363	1730	36.64	90.05	15	124	78	152	1.1E+23	(1,2)
081465	1313	37.22	89.31	1.5	280	70	-20	2.9E+21	(1,2)
102165	0204	37.48	90.94	5	260	40	-70	9.0e+22	(1,2)
072167	0914	37.44	90.44	15	350	60	-45	1.3E+22	(1,2)
110968	1701	37.91	88.37	22	0	46	79	9.7E+23	(1,2)
111770	0213	35.86	89.95	16	220	75	150	1.6E+22	(1,2)
040374	2305	38.55	88.07	15	310	70	0	3.7E+22	(1,2)
061375	2240	36.54	89.68	9	85	60	-20	4.6E+21	(1,2)
032576	0041	35.59	90.48	12	220	65	150	9.8E+22	(1,2)
061087	2348	38.71	87.95	10	135	70	15	3.1E+23	(3)
092690	1318	37.16	89.58	15	140	75	50	3.0E+22	(4)
050491	0118	36.56	89.83	8	90	67.5	20	1.8E+22	(4)
Revisions This Paper									
030363	1730	36.64	90.05	15	304	78	-28	1.1E+23	(4)
072167	0914	37.44	90.44	15	350	60	135	1.3E+22	(4)

(1) Origin time and location from Gordon (1988)
(2) Depth, seismic moment and mechanism from Herrmann (1979)
(3) Taylor *et al.* (1989)
(4) This paper

Table 10
Earth Models Used for Regional Modeling

H	α	β	ρ	Q_α^{-1}	Q_β^{-1}
CUS					
1.00	5.00	2.89	2.5	.0050	.010
9.00	6.10	3.52	2.7	.0005	.001
10.00	6.40	3.70	2.9	.0005	.001
20.00	6.70	3.87	3.0	.0005	.001
---	8.15	4.70	3.4	.0005	.001
MALDEN					
1.00	4.89	2.83	2.5	.0050	.010
9.00	5.98	3.44	2.7	.0005	.001
10.00	6.21	3.59	2.8	.0005	.001
10.00	6.44	3.72	2.8	.0005	.001
10.00	6.47	3.74	2.8	.0005	.001
20.00	7.97	4.60	3.3	.0005	.001
---	8.05	4.65	3.3	.0005	.001

In conclusion, waveform modeling of broadband data provides an extra constraint, and perhaps even a very sharp constraint on focal mechanisms.

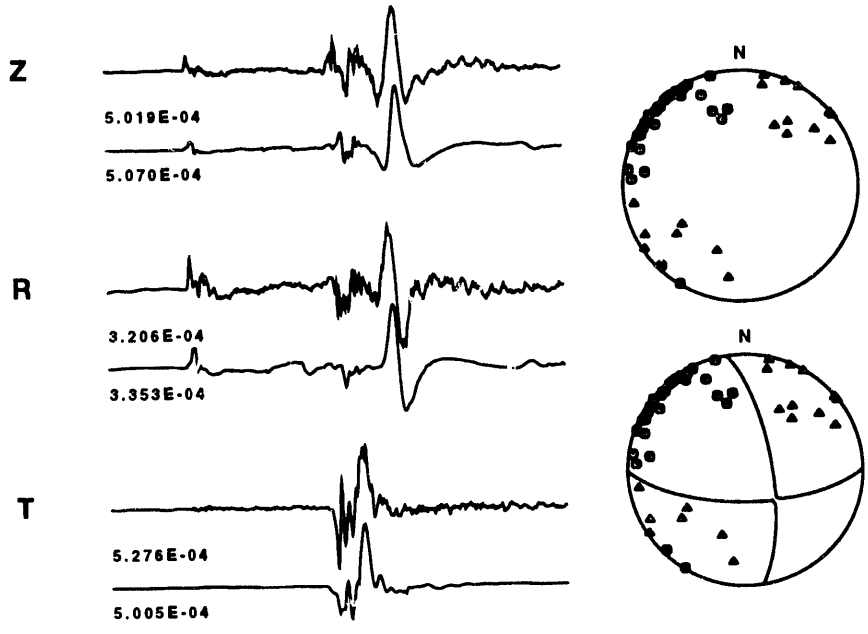

Fig. 30. Comparison of observed and synthetic (upper and lower traces, respectively, for each component) time histories for the May 4, 1991 earthquake recorded at the IRIS station CCMV. Both sets are passed through a 15-100 WWSSN LP instrument response with a peak gain of 1. A total of 80 seconds of time history is displayed, starting 20 seconds after the event origin time. The lower hemisphere equal area projections to the right show the observed P-wave first motion data from the event with (upper) and without (lower) the focal mechanism superimposed. Circles and triangles indicate compressional or dilatational P-wave first-motion, respectively.

REGIONAL STRESS PATTERNS

It is now widely accepted that the regional compressional stress field in the central U. S. is oriented in a ENE direction (Zoback and Zoback, 1991; Zoback, 1992). Much of the stress information in this region is based on earthquake focal mechanisms based on fits to surface-wave spectral amplitude radiation patterns (Herrmann, 1974; Herrmann, 1979; Taylor *et al.*, 1989). There are some exceptions to this stress pattern. Zoback (1992) notes that two published focal mechanisms in the region have normal faulting (October 21, 1965; July 21, 1967) and one has a pressure axis trending NS rather than EW (March 3, 1963), and are thus inconsistent with the inferred midcontinent stress patterns.

The focal mechanisms for these events are taken from Herrmann (1974, 1979) who analyzed surface-wave spectral amplitude radiation patterns. A systematic search of the strike, dip, rake, and source depth parameter space was performed to find a suite of solutions having a best fit to the spectral amplitudes. Because only fundamental mode surface wave data were used, there was an inherent ambiguity of 180° in strike, due to the symmetry of the theoretical radiation patterns. In addition, since amplitude data were used, the compressional and dilatational quadrants could only be defined with the

use of independent P-wave first motion data.

For many of the earthquakes, the quality of the P-wave first motion data was marginal. Eventually, the author learned to place more faith in the surface-wave constraints and to use only those P-wave first motions which were very impulsive. Herrmann (1979) attempted to test the quality of a solution by comparing the observed and predicted surface-wave phase at selected periods. For the three events indicated above, the phase agreement was not good.

Resolution of this problem is possible if broadband modeling is used. A simple null test is proposed. *Do the published focal mechanisms of Herrmann (1979) yield synthetic seismograms that match nearby long period seismograms?* To do this, the seismic moment, source depth and basic focal mechanism are not changed. The strike can be incremented by 180° and the pressure and tension axes interchanged. Neither affects the spectral amplitude radiation patterns.

Figure 31 shows the location of the seismograph stations providing waveforms as well as the earthquakes studied. The published focal mechanism parameters are assembled in Table 9.

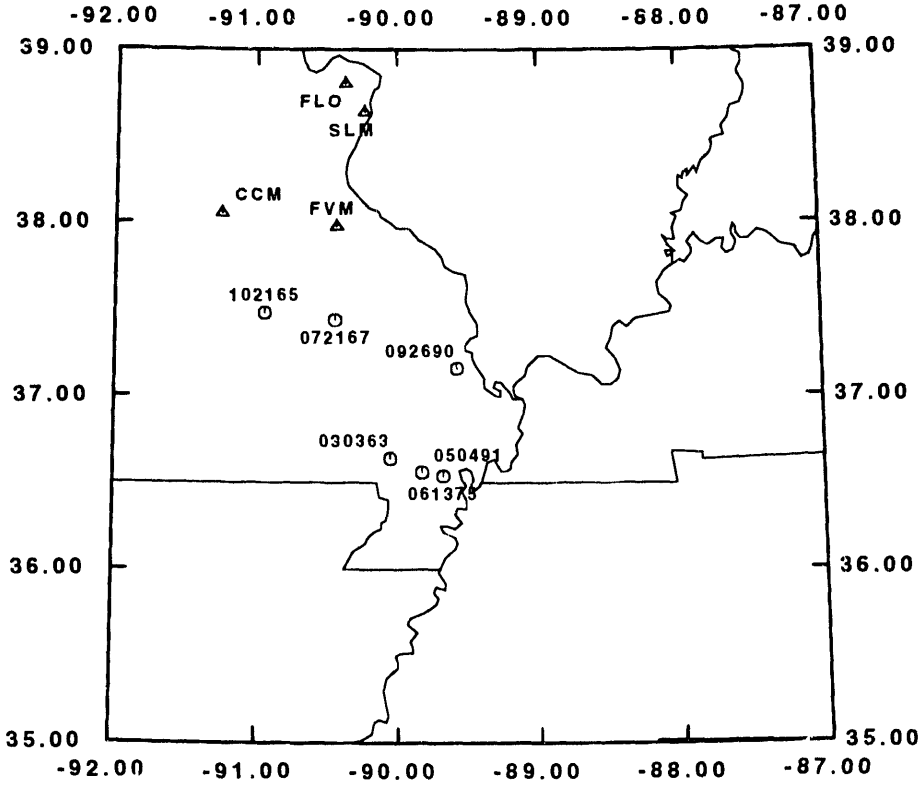

Fig. 31. Locations of seismograph stations CCM, FLO, FVM and SLM (triangles), and locations of events whose waveforms were analyzed (indicated by the circles and the dates).

March 3, 1963

Of the ten earthquakes studied by Herrmann (1974), this event had the greatest number of observations, and also the best observed and fit radiation patterns. Figure 42 compares the observed

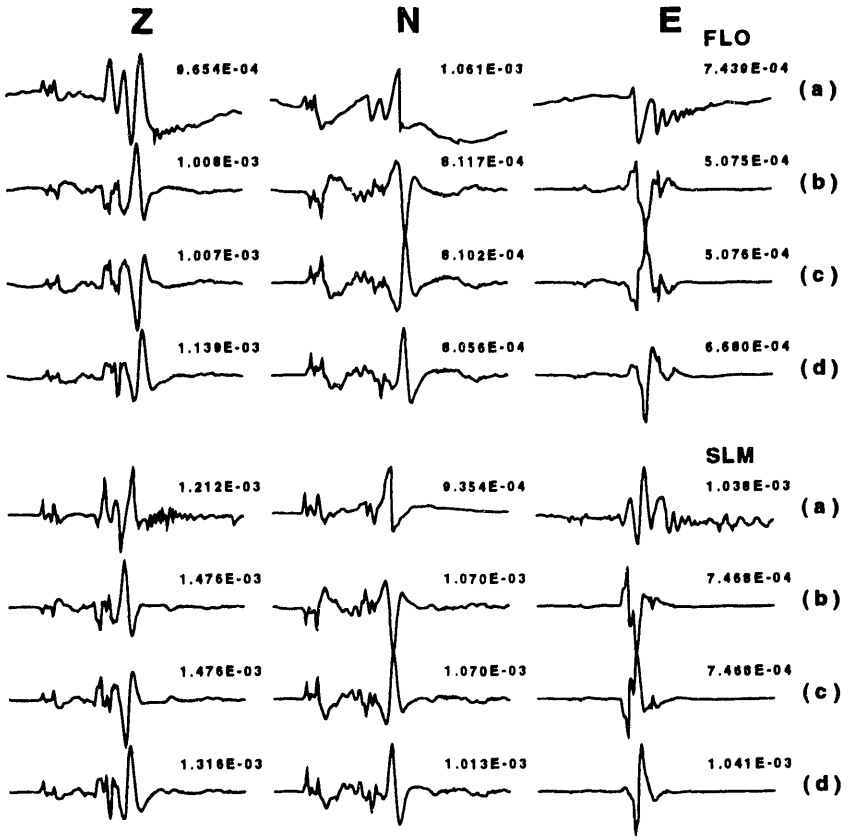

Fig. 32. Comparison of time histories at FLO (top) and SLM (bottom) for the March 3, 1963 earthquake. In each display, the digitized trace is indicated by (a), the trace predicted on the basis of the published focal mechanism by (b), the trace for the same nodal planes but with P- and T-axes interchanged by (c), and the trace with the nodal planes rotated by 180° and the P- and T-axes interchanged by (d). The time histories start 20 seconds after the origin time. A total of 102.2 seconds is displayed. FLO is 235 km at an azimuth of 354° form the source, and SLM is 215.48 km along an azimuth of 357°. Peak trace amplitudes are in cm units for a peak instrument magnification of 1.0. Positive Z, N and E values, indicate motion up, north and east.

and predicted long period seismograms at FLO and SLM. At this time FLO had a 30-100 WWSSN long-period response, and SLM had an approximately a 15-100 WWSSN response. Both the observed and synthetic traces have been adjusted for a peak instrument gain of 1.0. Given the quality of these long period seismograms close to regional earthquakes of magnitude 5, no attempt was made to rotate the components to form radial and transverse time histories.

In this figure, (a) represents the observed time history and (b) represents the synthetic predicted from the previously published mechanism (Table 9). It is very obvious that the polarity of the P-wave motion on the Z and N components is incorrect. The traces annotated by (c) have the same nodal planes but with interchanged P- and T-axes. This corrects the P-wave motion, but gives the wrong initial motion on the E component at FLO. Finally the traces indicated by (d) are due to an interchange of the P- and T-axes as well as a rotation of the nodal planes by 180°. This provides a better fit to the FLO E component, and a superposition of traces at both stations, indicates that (d) is preferred to (c). This revised mechanism is given in the lower half of Table 9.

The important result is that the P- and T- axes must be interchanged. The P-wave first motion data of this event were reexamined, and care was taken to use only those data having impulsive arrivals. This culled data set had fewer inconsistencies with (d) than with (c) and of course many fewer than with the original mechanism.

October 21, 1965

This event was studied by Mitchell (1973), Herrmann (1974, 1979), and Patton (1976). All authors agree that this event was shallow, ~5 km, and that motion was on a roughly east-west striking normal fault. The comparison of observed and predicted traces in Figure 33, shows agreement in the sense of the

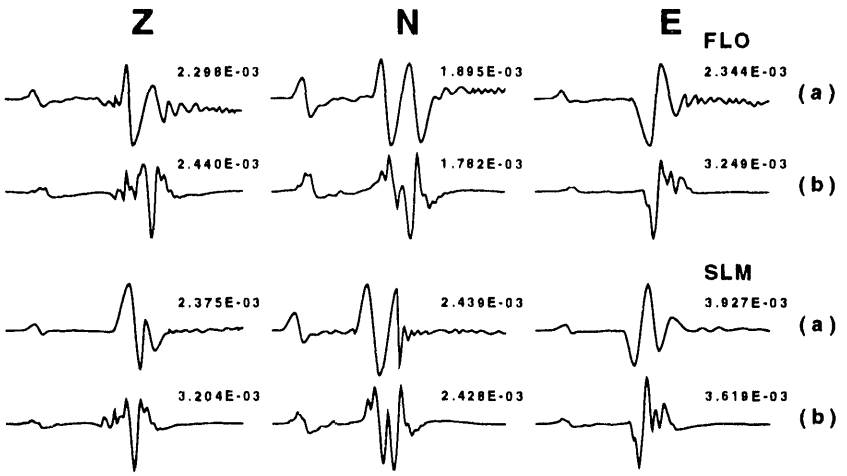

Fig. 33. Comparison of time histories for the October 21, 1965 earthquake recorded at FLO and SLM: (a) observed seismogram and (b) is the prediction based on the parameters of Table 9. The traces start 20 seconds after the origin time and 51.0 seconds of time history are plotted. The station FLO is 155 km from the event along an azimuth of 21° and the station SLM is 143 km from the event along an azimuth of 28°. Both instruments have WWSSN 15-100 LP responses and a peak gain of 1.0.

P-wave fist motion at the two stations, and rough agreement in the sense of

SH motion on the E-W component. The different frequency content, may indicate the need for a slightly deeper depth. However, the published focal mechanism is not contradicted by the waveform fit. Although this mechanism is that of a normal fault, the null axis is in the E-W direction. As was suggested by Mitchell *et al.* (1991), this interchange of axes may be due to local regional uplift.

July 21, 1967

Figure 34 compares the digitized traces at FLO and SLM (a) with the

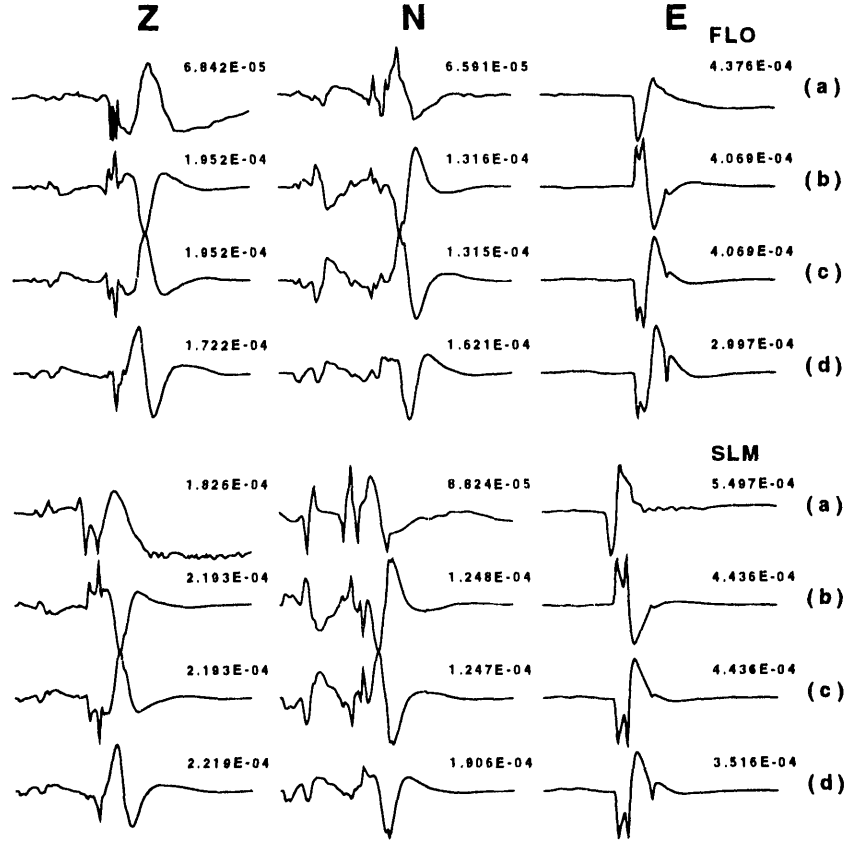

Fig. 34. Comparison of time histories for the July 21, 1967 earthquake recorded at FLO and SLM: (a) observed time histories, (b) prediction based on published mechanism, (c) prediction with published nodal planes but with P- and T-axes interchanged, and (d) prediction with nodal plane strike incremented by 180° and the P- and T- axes interchanged. FLO is 145 km from the event along an azimuth of 1°, and SLM is 127 km away along an azimuth of 6°. The traces start at 20 seconds after the event origin and continue for 51.0 seconds. Both instruments have WWSSN 15-100 LP responses and a peak gain of 1.0.

predictions based on the published mechanism (b). It is obvious that the SH pulse on the E component disagrees with the observed data, as does dome of the P-wave character on the Z and N components. This is a small event, and the maximum trace amplitude on the original data was at most several

millimeters. If the original nodal planes are kept, but the P- and T- axes are interchanged, the traces given by (c) result. These fit the observed data much better. The result further changing the nodal plane strike by 180° (d) yields pulse shapes that do not fit the Rayleigh wave as well. The conclusion is that the published mechanism should be revised as indicated in the last entry in Table 9.

June 13, 1975

This event was discussed by Herrmann *et al.* (1977) and its source parameters are well constrained by surface-wave and regional seismic network data. The reason that this event is considered here is not to verify the focal mechanism, but to test the published seismic moment. This is because this event provided an analog strong motion record within 10 km of the event, and because this event occurred very close to the location of the May 4, 1991 which triggered a nearby digital strong motion recorder (Friberg *et al*, 1991). Using the Friberg *et al* (1991) corner frequency of 3.0 ± 0.2 Hz and the seismic moment of 1.8 x 10^{22} dyne-cm presented here, the inferred stress drop of the 1991 earthquake would be 100 bars. The 1975 event corner frequency is in the range of 2 - 3 Hz (Z. Liu, personal communication; Herrmann *et al.*, 1977) and its published seismic moment of 4.6 x 10^{21} dyne-cm, would imply a stress drop four times less. Thus the interest in the seismic moment is related to demonstrating variability in stress drop for at least two nearby earthquake in the region.

Figure 35 compares the observed and predicted time histories at FVM for this event.

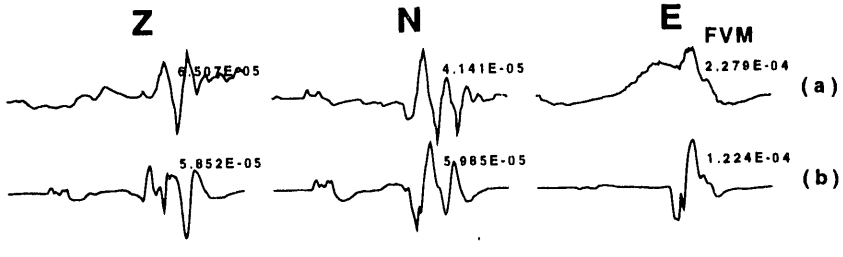

Fig. 35. Comparison of time histories for the June 13, 1975 earthquake recorded at FVM: (a) observed time history and (b) predicted time history using the parameters of Table 9. The instrument has WWSSN 15-100 LP responses and a peak gain of 1.0. The time histories start 20 seconds after the event and continue for 51.0 seconds. FVM is a distance of 177 km along an azimuth of 339° from the event. Because of the long period noise, both synthetics and observed data were also high pass filtered using a Butterworth filter with a corner frequency of 0.04 Hz.

The agreement in waveform shape and amplitude is excellent, indicating that the previously obtained surface-wave seismic moment can explain this data set at a relatively short epicentral distance. Thus the possibility of a stress drop less than 100 bars can not be rejected, with the cautionary note that the

stress drop is very sensitive to the choice of corner frequency.

DISCUSSION

This paper introduced a novel, but certainly reasonable use of broadband waveform modeling to simply verify some published focal mechanisms. Only a few traces were used because of the desire to use waveform data at distances less than 200 km so that inaccuracies in crustal model would not be too severe in their affect on synthetic seismograms. The results of this paper show that the published focal mechanisms for the March 3, 1963 and the July 21, 1967 earthquakes are incorrect in their choice of compressional and dilatational quadrants. The modification of these two mechanisms can be justified in that they were not really well constrained by the low quality P-wave first motion data used at the time. The author has since learned to rely solely on just a few, very impulsive P-wave first arrivals to define the orientation of the pressure and tension axes.

Figures 36 and 37 overlay the corrected and other acceptable focal mechanisms on the regional microearthquake seismicity catalog for the time period 1975 - 1992. Figure 36 covers the larger geographical area of 4° in latitude and and 5° in longitude, while Figure 37 focuses in on a region of 2° in latitude and 1.5° in longitude.

As can be seen from these figures, with the exception of the October 21, 1965 earthquake, the focal mechanism P-axes typically trend in a ENE direction, in agreement with the broad central U. S. pattern observed in all stress indicators by Zoback (1992). Figure 37 is interesting in that the March 3, 1963 earthquake lines at the end of a WNW trending seismicity pattern emanating from the NNW seismicity trend at New Madrid. In addition, one of the nodal planes of the event can be associated with the seismicity trend, and thus may be identified as the fault plane. The observed seismicity terminates at the lower left corner of the plot. It is interesting that both the March 25, 1976 and the March 3, 1963 earthquakes both occurred at the end of linear seismicity trends and that these were the largest earthquakes, $M_0 \approx 10^{23}$, in this mapped region during the last 30 years.

One final point is that even though there is a wealth of information in modern broadband data, the waveform fit to the analog data was not pursued in greater detail than the simple comparison presented because of the low signal levels and the difficulty of digitizing seismograms with the necessary accuracy to permit the waveform to be thoroughly analyzed.

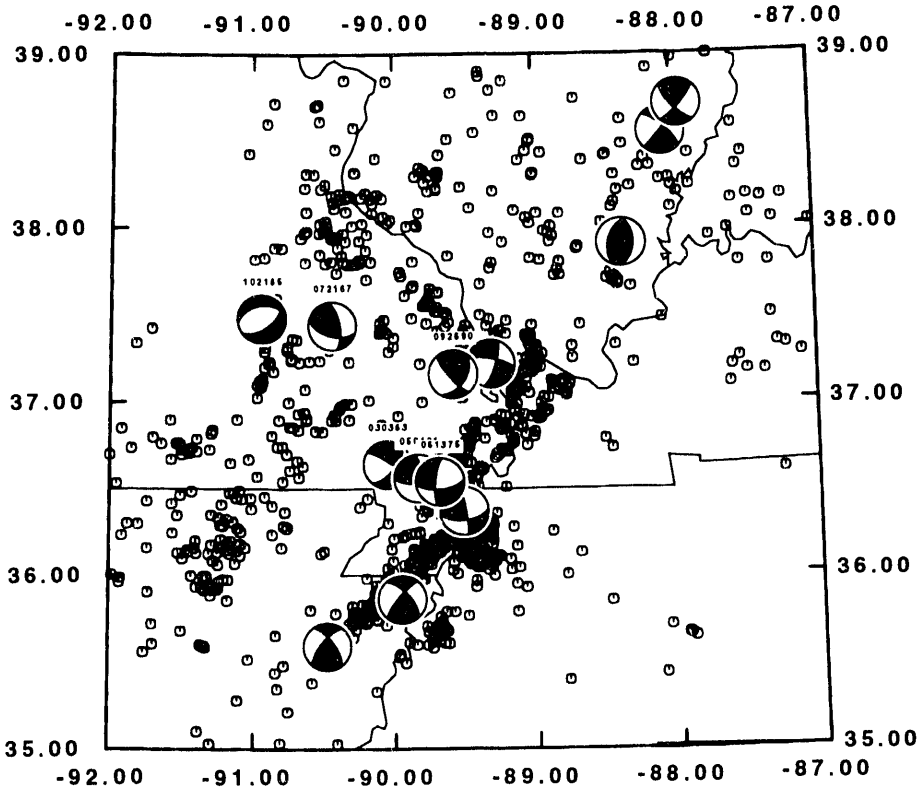

Fig. 36. Regional seismic network earthquake locations for 1975 - 1992 together with accepted focal mechanisms. The compressional quadrants are shaded. A lower hemisphere, equal are projection is used.

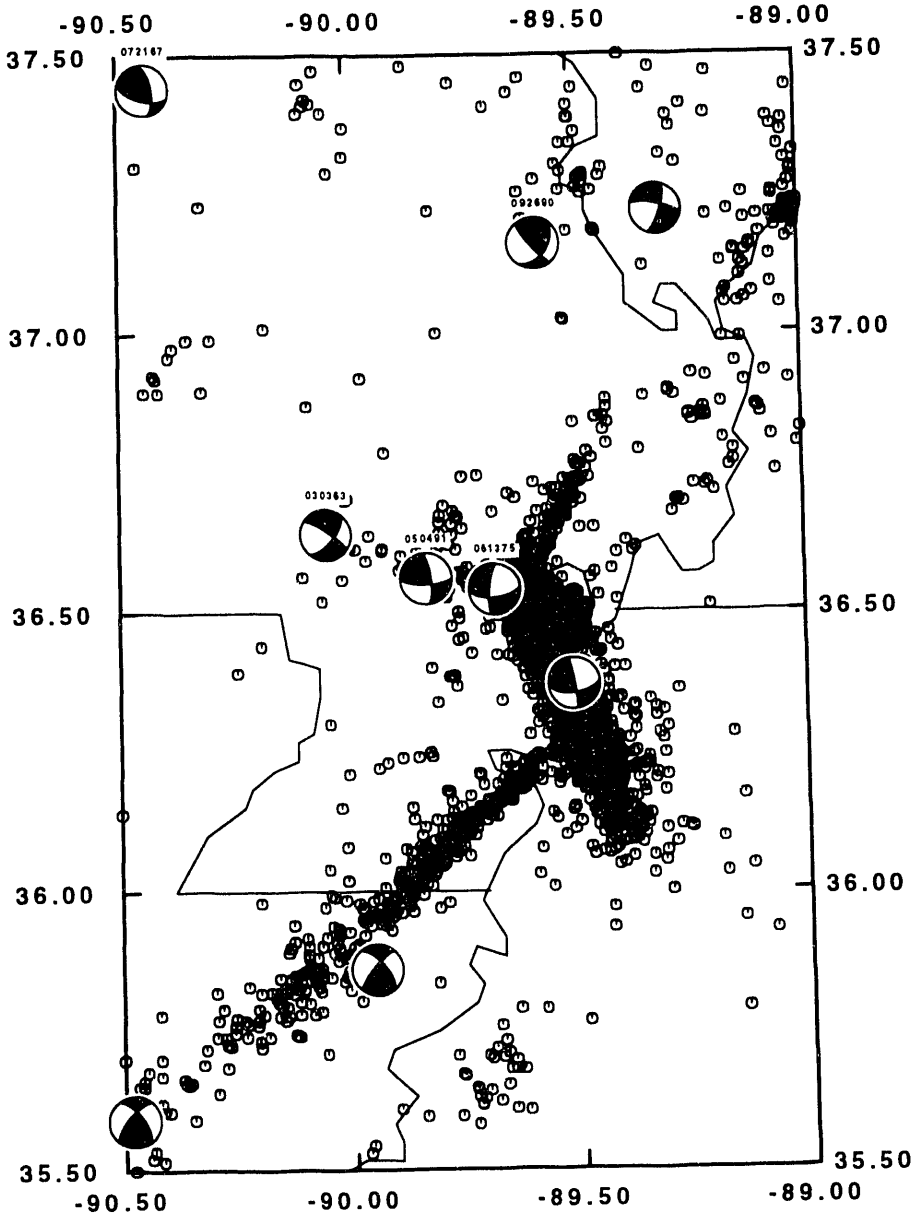

Fig. 37. Regional seismic network earthquake locations for 1975 - 1992 together with accepted focal mechanisms. This plot focuses on the linear seismicity trends of the New Madrid Seismic Zone. The compressional quadrants are shaded. A lower hemisphere, equal are projection is used.

SEISMIC NETWORK RESULTS

Robert B. Herrmann

DISCUSSION

The result of monitoring the earthquake process in the New Madrid Seismic Zone from July, 1974 - June, 1992 is shown in Figures 36 and 37. Figure 36 gives the location of over 3700 earthquakes in a 5° x 4° region, while Figure 37 shows the location of over 2800 events in a 1.5° x 2° subregion within fIGURE 36. The spatial patterns of the concentration of seismicity have been known from the initial deployment of the network (Stauder *et al.*, 1976). While the annual number of earthquakes is significantly less than for seismic networks in California, the activity rate is the highest and most persistent in the United States east of the Rocky Mountains.

The earthquake locations and phase data are being maintained online at Saint Louis University for future reference. In addition, the catalog of event locations and a computer based graphics display are available in on floppy disk for use on an IBM compatible PC.

More important for future research is the preservation of digitally acquired data. Since 1981, data from larger earthquakes have been acquired digitally on a series of computers. These triggers yielded about 1500 teleseisms and 1500 local earthquakes fro the time period 1981 - 1992. These data were originally archived on a dual pair magnetic tapes. However, through time, the value of these recordings decreases as the digital data deteriorates. All teleseism and about one-half of the earthquake data have been data have been transferred from magnetic tape to optical disk, with the remainder being transferred now. In addition, instrument calibrations for the digital data are being finalized, so that the final archive will be a complete data set for future use in source and ground motion studies. These data may eventually be deposited in the IRIS data base for permanent archiving.

Through U. S. Geological Survey support, the earthquake process within the region is continues to be monitored and the monitoring equipment is being modernized. Thus data will continue to be acquired from this significant seismic zone that will be available to the U. S. Nuclear Regulatory Commission for its needs.

REFERENCES

Ben-Menahem, A., H. Jarosch, and M. Rosenman (1968). Large scale processing of seismic data in search of regional and global stress patterns, *Bull. Seism. Soc. Am.* **58,** 1899-1932.

Birch, F. (1964). Density and composition of mantle and core, *J. Geophys. Res.* **69,** 4377-4388.

Bullen, K. E. and B. A. Bolt (1985). *An Introduction to the Theory of Seismology,* Cambridge University Press, Cambridge, 499 pp.

Chiu, J.M., A.C. Johnston, A. G. Metzger, L. Haar, and J. Fletcher (1984). Analysis of analog and digital record of the 1982 Arkansas earthquake swarm, *Bull. Seism. Soc. Am.* **74,** 1721-1742.

Choy, G. L., J. Boatwright, J. W. Dewey, and S. A. Sipkin (1983). Teleseismic analysis of the New Brunswick earthquake of January 9, 1982, *J. Geophys. Res.* **88,** 2199-2212.

Dreger, D. S., and D. V. Helmberger (1991). Complex faulting deduced from broadband modeling of the 28 February 1990 Upland earthquake, ($M_L = 5.2$), *Bull. Seism. Soc. Am.* **81,** 1129-1144.

Dreger, D. S., and D. V. Helmberger (1993). Determination of source parameters at regional distances with three-component sparse network data, *J. Geophys. Res.* **98,** 8107-8125.

Dziewonski, A., S. Block, and M. Landisman. (1969). A technique for the analysis of transient seismic signals, *Bull. Seism. Soc. Am.* **59,** 427-444.

Dziewonski, A. M. and J. H. Woodhouse (1983). An experimental systematic study of global seismicity: Centroid-moment tensor solutions for 201 moderate and large earthquakes of 1981, *J. Geophys. Res.* **88,** 3247-3271.

Ebel, J. E. and B. R. Bouck (1988). New focal mechanisms for the New England region: Constraints on the regional stress regime, *Seism. Res. Lett.* **59,** 183-187.

Foley, J. E., G. Buzzell, C. Doll, M. Dollin, F. Filipkowski, M. B. Hulit, J. P. McCaffrey, S.J., and V. Vudler (1982). *Seismicity of the Northeastern United States, Bulletin No.* **26,** Weston Observatory, Boston College.

Friberg, P., K. Jacob, and S. Hough (1991). Analysis of strong-motion data from the Malden, Missouri earthquakes of May 4, 1991 (abs), *Seism. Res.*

Letters **62,** 170.

Gordon, D. W. (1988) Revised instrumental hypocenters and correlation of earthquake locations and tectonics in the central United States, *U. S. Geological Survey Prof. Paper* **1364,** U. S. Government Printing Office, Washington, 69 pp.

Hasegawa, H. S. (1983). Surface waves analysis of the magnitude 5.7 Miramichi, New Brunswick, earthquake of 09 January 1982 (abs), *Earthquake Notes* **54,** No. 1., 84.

Herrin E., *et al.* (1968). 1968 Seismological Tables for P Phases, *Bull. Seism. Soc. Am.* **58,** 1193-1225.

Herrmann, R. B. (1973). Some aspects of band-pass filtering of surface waves, *Bull. Seism. Soc. Am.* **63,** 663-671.

Herrmann, R. B. (1974). Surface wave generation by central United States Earthquakes, *Ph.D. Dissertation,* Saint Louis University, 263pp.

Herrmann, R. B. (1979a). Surface-wave focal mechanisms for eastern North American earthquakes with tectonic implications, *J. Geophys. Res.* **84,** 3543-3552.

Herrmann, R. B. (1979b). FASTHYPO -- A hypocenter location program, *Earthquake Notes* **50,** No. 2., 25-37.

Herrmann, R. B. (1979c). SH-wave generation by dislocation sources -- a numerical study, *Bull. Seism. Soc. Am.* **69,** 1-15.

Herrmann, R. B. and B. J. Mitchell (1975). Statistical analysis and interpretation of surface-wave anelastic attenuation data for the stable interior of North America, *Bull. Seism. Soc. Am.* **65,** 1115-1128.

Herrmann, R. B., G. W. Fischer, and J. E. Zollweg (1977). The June 13, 1975 earthquake and its relationship to the New Madrid Seismic Zone, *Bull. Seism. Soc. Am.* **67,** 209-218.

Herrmann, R. B., J. W. Dewey, and S. K. Park (1980). The Dulce, New Mexico earthquake of 23 January 1966, *Bull. Seism. Soc. Am.* **70,** 2171-2184.

Herrmann, R. B. and B. V. Nguyen (1988). Source parameters of the northeastern Ohio earthquake of 31 January 1986, in *Seismological Investigation of Earthquakes in the New Madrid Seismic Zone and the Northeastern Extent of the New Madrid Seismic Zone, September 1981-December 1986,*

Final Report NUREG/CR-5165, R. B. Herrmann, K. Taylor and B. Nguyen, eds., Department of Earth and Atmospheric Sciences, St. Louis University, prepared for U.S. Nuclear Regulatory Commission, 44 pp.

Hildenbrand, T. G., J. G. Rosenbaum and R. L Reynoled (1992). high-resolution aeromagnetic study of the New MAdrid Seismic Zone: a preliminary report, *Seism. Res. Letters* **63,** 209-232.

Jenkins, G. M., and D. G. Watts (1968). *Spectral Analysis and Its Applications*, Holden-Day, San Francisco.

Johnston, A. C. (1982). Arkansas's earthquake laboratory, *EOS, Trans. Am. Geophys. Union* **63,** 1209-1210

Langer, C. J. (1985). Seismological Field Investigations, in *USGS, National Earthquake Hazards Reduction Program, Summaries of Technical Reports, Vol. XX, July 1985. Open File Report 85-464,* 17.

Liu, Z., R. B. Herrmann, J. Xie, and E. Cranswick (1991). Waveform characteristics and focal mechanism solutions of five aftershocks of the 1983 Goodnow, New York, earthquake by polarization analysis and waveform modeling, *Seism. Res. Letters* **62,** 123-133.

Mitchell, B. J. (1973). Radiation pattern and attenuation of Rayleigh waves from the southeastern Missouri earthquake of October 21, 1965 , *J. Geophys. Res.* **78,** 886-899.

Mitchell, B. J., O. W. Nuttli, R. B. Herrmann, and W. Stauder (1991). Seismotectonics of the central United States, in *Neotectonics of North America,* D. B. Slemmons, E. R. Engdahl, M. D. Zoback and D. D. Blackwell, eds., Geological Society of America, Boulder, pp 245-260.

Mrotek, K. A., C. T. Statton, J. D. Agnew, P.G. Naumoff, R. C. Quittmeyer, G. LeBlanc, and G. Klimkiewicz (1986). Aftershock survey of the Northeastern Ohio earthquake of 31 January 1986 (abs), *EOS, Trans. Am. Geophys. Union* **67,** 314.

Nábelek, J. (1985). The January 9, 1982, New Brunswick, Canada earthquake, in *A Study of New England Seismicity With Emphasis on Massachusetts and New Hampshire, Technical Report covering 1982-1984,* Earth Resources Laboratory, Massachusetts Institute of Technology, 104pp.

Nábelek, J. and G. Suarez (1989). The 1983 Goodnow earthquake in the central Adirondacks, New York: Rupture of a simple, circular crack, *Bull.*

Seism. Soc. Am. **79,** 1762-1777.

Nguyen, B. V. (1985). Surface-wave focal mechanisms, magnitudes, and energies, for some eastern North-American earthquakes with tectonic implication, *M.S. Thesis,* Saint Louis University, 275pp.

Nguyen, B. V. (1988). Determination of earthquake source parameters from search procedure and from moment tensor inversion of surface waves. *Ph.D. Dissertation,* Saint Louis University, 202pp.

Nicholson, C., E. Roeloffs, and R. L. Wesson (1988). The northeastern Ohio earthquake of 31 January 1986: Was it induced?, *Bull. Seism. Soc. Am.* **78,** 188-217.

Nuttli, O. W., W. Stauder, and C. Kisslinger (1969). Travel time tables for earthquakes in the central United States, *Earthquake Notes* **40,** No. 4, 19-28.

Patton, H. (1976). A note on the source mechanism of the southeastern Missouri earthquake of October 21, 1965, *J. Geophys. Res.* **81,** 1483-1486.

Pulli, J. J., J. L. Nábelek, and J. M. Sauber (1983). Source parameters of the January 19, 1982 Gaza, NH earthquake (abs), *Earthquake Notes* **54,** No. 3., 28.

Russell, D. R., R. B. Herrmann, and H. J. Hwang (1988). Application of frequency variable filters to surface-wave amplitude analysis, *Bull. Seism. Soc. Am.* **78,** 339-354.

Saikia, C. K., and R. B. Herrmann (1986). Moment-tensor solutions for three 1982 Arkansas swarm earthquakes by waveform inversion, *Bull. Seism. Soc. Am.* **76,** 709-723.

Sauber, J. M. (1985). The January 19, 1982 Gaza, New Hampshire earthquake, in *A Study of New England Seismicity With Emphasis on Massachusetts and New Hampshire, Technical report covering 1982-1984,* Earth Resources Laboratory, Massachusetts Institute of Technology, 104pp.

Seeber, L. and J. G. Armbruster (1986). *A Study of Earthquake Hazards in New York State and Adjacent Areas, Final Report Covering the Period 1982-1985, Report to the Nuclear Regulatory Commission, NUREG/CR-4750, Washington, D.C.*

Shumway, R. H. (1988). *Applied Statistical Time Series Analysis,* Prentice-

Hall, Englewood Cliffs.

Stauder, W., M. Kramer, G. Fischer, S. Schaefer, and S. T. Morrissey (1976). Seismic characteristics of southeast Missouri as indicated by a regional telemetered microearthquake array, *Bull. Seism. Soc. Am.* **66,** 1953-1964.

Suarez, G. and J. Nábelek (1983). The January 9, 1982 New Brunswick earthquake: A moment tensor inversion from the amplitude spectra of Rayleigh waves (abs), *Earthquake Notes* **54,** No. 3., 34.

Suarez, G., L. Seeber, C. Aviles, E. Schlessinger-Miller, and J. L. Nábelek (1984). The Goodnow, NY earthquake: results from a broad-band teleseismic analysis (abs), *EOS, Trans. Am. Geophys. Union* **65,** 239-240.

Talwani, M., G. H. Sutton, and J. L. Worzel (1959). Crustal section across the Puerto Rico Trench, *J. Geophys. Res.* **64,** 1545-1555.

Tarr, A. C. (1985). Source properties of Great Basin earthquakes, in *USGS, National Earthquake Hazards Reduction Program, Summaries of Technical Reports, Vol. XXI, October 1985, Open-File Report 86-31,* 515-516.

Taylor, K. B., R. B. Herrmann, ... W. Hamburger, G. L. Pavlis, A. Johnston, C. Langer, and C. Lam (1989). The southeastern Illinois earthquake of 10 June 1987, *Seism. Res. Letters* **60,** 101-110.

Taylor, K. B., and M. E. Wuenscher (1990). Special investigations of seismic activity: The Ripley, Tenn. earthquake of 29 Aug. 1990 and the New Hamburg, Missouri earthquake of 26 Sept. 1990, in *Central Mississippi Valley Earthquake Bulletin: Quarterly Bulletin 66, Third Quarter 1990,* Saint Louis University.

Toksöz, M. N. and J. J. Pulli (1984). Source and path effects for Northeastern U.S. earthquakes-Implications for earthquake hazards, in *USGS, National Earthquake Hazards Reduction Program, Summaries of Technical Reports, Vol. XIX, December 1984, Open-File Report 85-22,* 550-554.

Tsai, Y. B. (1972). Use of LP surface waves for source characterization, *Geophys. J.* **31,** 111-130.

Tsai, Y. B. and K. Aki (1969). Simultaneous determination of seismic moment and attenuation of surface waves, *Bull. Seism. Soc. Am.* **59,** 275-287.

Tsai, Y. B. and K. Aki (1970). Precise focal depth determination from amplitude spectra of surface waves, *J. Geophys. Res.* **75,** 5729-5743.

Wetmiller, R. J., F. M. Anglin, H. S. Hasegawa, and A. E. Stevens (1984). Aftershock sequences of the 1982 Miramichi, New Brunswick, earthquakes, *Bull. Seism. Soc. Am.* **74,** 621-653.

Yan, B. and S. S. Alexander (1990). Source mechanism study of the 1982 New Brunswick, Canada, earthquake sequence using combined surface-wave methods, *Bull. Seism. Soc. Am.* **80,** 296-312.

Zoback, M. L. and M. Zoback (1980). State of stress in the conterminous United States, *J. Geophys. Res.* **85,** 6113-6156.

Zoback, M. D., and M. L. Zoback (1991). Tectonics stress field of North America and relative plate motions, in *Neotectonics of North America,* D. B. Slemmons, E. R. Engdahl, M. D. Zoback and D. D. Blackwell, eds., Geological Society of America, Boulder, pp 339-366.

Zoback, M. L. (1992). Stress field constraints on intraplate seismicity in eastern North America, *J. Geophys. Res.* **97,** 11761-11782.

DATE
FILMED
10 / 14 / 93
END